Baseline studies of surface gas exchange and soil-gas composition in preparation for CO_2 sequestration research: Teapot Dome, Wyoming

Ronald W. Klusman

ABSTRACT

A baseline determination of CO_2 and CH_4 fluxes and soil-gas concentrations of CO_2 and CH_4 was made over the Teapot Dome oil field in the Naval Petroleum Reserve 3 in Natrona County, Wyoming, United States. This was done in anticipation of the experimentation with CO_2 sequestration in the Pennsylvanian Tensleep Sandstone underlying the field at a depth of 5500 ft (1680 m). The measurements were made in January 2004 to capture the system with minimum biological activity in the soils, resulting in a minimum CO_2 flux and a maximum CH_4 flux. The CO_2 fluxes were measured in the field with an infrared spectroscopic method. The CH_4 fluxes were determined from gas-chromatographic measurements on discrete samples from under the flux chambers. The CO_2 and CH_4 were determined at 30-, 60-, and 100-cm (11-, 23-, and 39-in.) depths in soil gas by gas chromatography. A total of 40 locations had triplicate flux measurements using 1.00-m^2 (10.763-ft^2) chambers, and soil gas was sampled at single points at each of the 40 locations.

Carbon dioxide fluxes averaged 227.1 mg CO_2 m^{-2} day^{-1}, a standard deviation of 186.9 mg m^{-2} day^{-1}, and a range of -281.7 to 732.9 mg m^{-2} day^{-1}, not including one location with subsurface infrastructure contamination. Methane fluxes averaged 0.137 mg CH_4 m^{-2} day^{-1}, standard deviation of 0.326 mg m^{-2} day^{-1}, and a range of -0.481 to 1.14 mg m^{-2} day^{-1}, not including the same contaminated location.

Soil-gas CO_2 concentrations increased with depth, averaging 618, 645, and 1010 ppmv at 30, 60, and 100 cm (11, 23, and 39 in.),

Copyright ©2005. The American Association of Petroleum Geologists. All rights reserved.

Manuscript received October 18, 2004; provisional acceptance November 17, 2004; revised manuscript received March 29, 2005; final acceptance March 31, 2005.

DOI:10.1306/03310504109

AUTHOR

RONALD W. KLUSMAN ~ *Department of Chemistry and Geochemistry, Colorado School of Mines, Golden, Colorado 80401; rklusman@mines.edu*

Ronald Klusman received a B.S. degree in chemistry and a Ph.D. in geology and geochemistry at Indiana University. During graduate studies, he was an instrumental analyst at the Indiana Geological Survey. From 1969 to 1972, he was an assistant professor of geosciences at Purdue University, and from 1972 to 2001, he was an associate professor and a professor of chemistry and geochemistry at the Colorado School of Mines. In 2001, he became professor emeritus, continuing research on a part-time basis.

ACKNOWLEDGEMENTS

This research was supported by the Rocky Mountain Oilfield Testing Center (RMOTC) of the U.S. Department of Energy under Contract No. PO03095 FY03 to the Colorado School of Mines. Vicki Stamp of RMOTC is the project manager. Advice, assistance, and cooperation of many individuals at RMOTC and the Naval Petroleum Reserve 3 were critical in making this research possible. Individuals from Isotech Laboratories, Inberg Miller Environmental Engineers, Colorado School of Mines, McCutcheon Energy Company, Lawrence Livermore National Laboratory, and reviewers of this manuscript (P. K. Mukhopadhyay, D. Schumacher, and L. L. Summa) also made valuable contributions.

respectively. Soil-gas CH_4 concentrations averaged 0.128, 0.114, and 0.093 ppmv at 30, 60, and 100 cm (11, 23, and 39 in.), respectively. The decrease in CH_4 with depth reflects a slow rate of methanotrophic oxidation, even during winter conditions. The $\delta^{13}C$ of the soil gas CO_2 was also determined in the soil-gas samples and in the atmosphere. These data demonstrated that the increased CO_2 with depth was derived from the biological oxidation of soil organic matter.

INTRODUCTION

Geological sequestration of CO_2 has been proposed for the reduction of the loading rate of anthropogenic CO_2 to the atmosphere. The Sleipner Vest project in the North Sea is an early prototype of this kind of a sequestration project, where the CO_2 content of a natural gas is reduced prior to delivery (Korbol and Kaddour, 1995). Sequestration in deep aquifers, coal beds, and depleted oil and gas fields has been proposed (van der Meer, 1993; van Engelenburg and Blok, 1993; Bachu et al., 1994; Hitchon et al., 1999; Bachu, 2000, 2002).

The sequestration of CO_2 in depleted oil and gas fields has dual benefits. Additional hydrocarbon recovery occurs, and substantial CO_2 is sequestered. In the case of a dual operational function, the most expensive part of the infrastructure is already in place, greatly improving the economics. The operation of a dual function field will have to be a compromise between two objectives, hydrocarbon production and CO_2 disposal. As the operation matures, and the field again becomes largely spent, sequestration will become the primary objective. At some point, the ability of the reservoir to transmit, contain, or chemically react with additional CO_2 will be maximized, and the operation shut in. Another important advantage is that the use of CO_2 in enhanced oil recovery (EOR) is a proven technology with more than 80 projects worldwide, contrasting with geological disposal. Blunt et al. (1993) described the CO_2-EOR from a nonpetroleum engineering perspective.

The U.S. Department of Energy owns and operates the Teapot Dome oil field in central Wyoming, which is part of the Naval Petroleum Reserve 3 (NPR-3) created in the 1920s (Figure 1). The Rocky Mountain Oilfield Testing Center does experimentation on the field. In 2003, NPR-3 was designated as a National Geologic Carbon Storage Test Site, with the primary objective of developing and testing new technologies supportive of CO_2 sequestration in the subsurface. The Department of Energy, being both the owner and operator of the field, allows for research and experimentation that might not be possible in a field operated primarily for EOR. The remote location of NPR-3 makes it ideal for experimentation with new subsurface technologies, without potential impact on privately owned surface property and structures. The field covers approximately 18 mi^2 (46 km^2) and has minor production from several stacked reservoirs. Anadarko Petroleum Corporation recently constructed a pipeline that is currently delivering CO_2 to the adjacent Salt Creek field, which is in the early phases of developing a CO_2-EOR operation (Figure 1). This pipeline will likely serve as a convenient source of CO_2 for future injection experimentation at NPR-3.

Purpose and Scope

A concern in any CO_2 sequestration operation is the potential for leakage into higher formations and to the surface (microseepage). Part of a larger monitoring operation must include the assessment of this potential and provide a program for early detection and quantification of microseepage rates over the period of operation.

The purpose of the study at NPR-3 is to provide a baseline survey of soil-gas composition and gas exchange with the atmosphere. The focus is on CO_2 and CH_4, both important greenhouse gases. These data can be used to study both the processes operating in the unsaturated zone, which are primarily biological production and consumption of gases, and possibly microseepage of gases from a deep source. This type of research attempts to detect and possibly quantify a weak, deep-sourced signal embedded in a larger, near-surface biological signal. Comparison of these data with future surveys after a period of CO_2 injection is anticipated. This preinjection survey contrasts with a comprehensive survey done at Rangely, Colorado, where CO_2-EOR has been operating since 1986 (Klusman, 2003b).

The injection of gases at the elevated pressure necessary to achieve acceptable rates poses some risk of leakage into adjacent and overlying formations and as microseepage to the surface. This may be caused by problems with preexisting or current infrastructure or migration along faults and fracture zones. Gases are

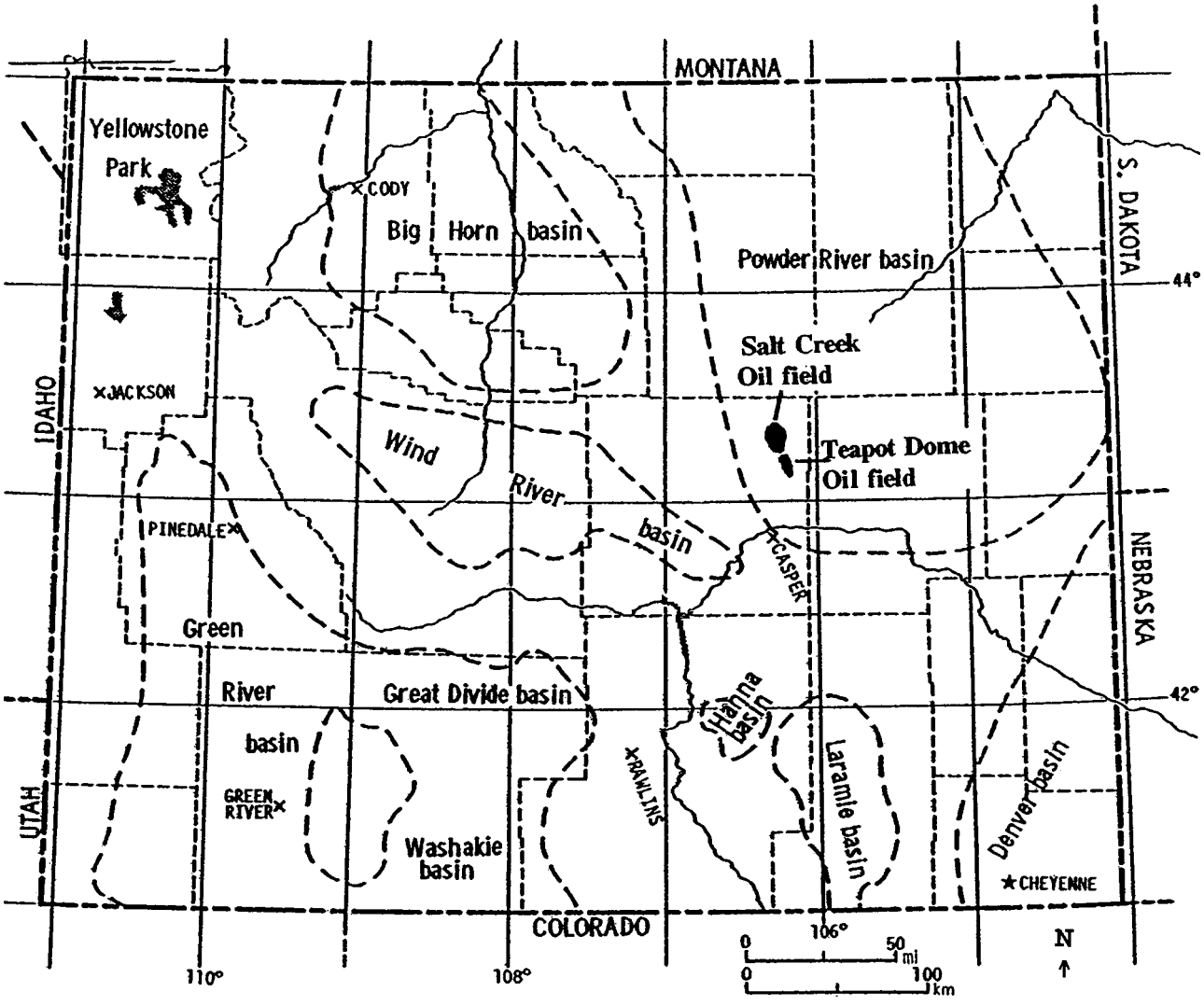

Figure 1. Location of Teapot Dome and Salt Creek oil fields in the southwestern Powder River basin, Wyoming (modified from Landes, 1970).

buoyant relative to a liquid hydrocarbon phase or a ground water. Overpressured systems are particularly susceptible to leakage as demonstrated by pressure-manipulated gas storage reservoirs used to meet seasonal variation in gas demand of metropolitan areas. The surface ownership of the Teapot Dome field by the Department of Energy allows for the open evaluation and publication of the microseepage potential and detection.

Methane is always present in oil fields being considered for EOR operations and in coalbed-methane operations, where it is the primary commodity for recovery. Because the gas behavior of CH_4 is much more ideal than CO_2 in the geologic environment, inclusion of CH_4 in studies of potential microseepage is critically important. Carbon dioxide is soluble in and reactive with water, whereas methane is not. Possible lateral or vertical migration of CO_2 will tend to be attenuated by the solubility in and reactivity with water.

Seasonality of Surface Measurements

Measurements of gas flux (exchange) with the atmosphere and in shallow soil gas will be dominated by biological processes operating in the soil, primarily root respiration and microbial oxidation of soil organic matter. These processes operate from the surface downward, with rates diminishing from the surface to barely detectable near the water table. Large seasonal variations exist, where the summer rates exceed the winter rates by a factor of 10 or more in a cold, dry climate

(Klusman, 2003a). In addition, methanotrophic oxidation of CH_4 (methanotrophy) occurs in the unsaturated zone. This process can use CH_4 from depth and/or CH_4 from the atmosphere. Because methanotrophy is also a biological process, the rate is largely determined by seasonal variation in soil temperature and moisture and the availability of the substrate, CH_4.

Sampling in the winter season will provide conditions closest to a baseline condition. Root respiration and microbial oxidation of soil organic matter will be at a minimum, as will methanotrophic oxidation of CH_4. Consequently, CO_2 fluxes to the atmosphere and soil-gas concentrations will be at a minimum, and CH_4 exchange with the atmosphere and soil-gas concentrations will be at a maximum.

Geology of Teapot Dome

The Teapot Dome field is an asymmetric anticline on the southwest corner of the Powder River basin (Figure 1). It is located in an en echelon position southeast of the larger Salt Creek field (Figure 2). The Teapot Dome and the Salt Creek field are two domes on a long, asymmetric anticline oriented northwest-southeast and formed by compression from the southwest (Thom and Spieker, 1931). Figure 2 shows the plan map of the NPR-3 with the Teapot Dome oil field centered in NPR-3 (Weitz and Harbison, 1954). The field is surrounded on three sides by sandstone hogbacks of the Parkman Sandstone Member of the Mesaverde Formation (Figure 3). Figure 4 shows the structure of the Teapot Dome using a crossline from a three-dimensional (3-D) seismic survey (McCutcheon, 2003).

During upward arching of the domal structure in NPR-3, numerous tensional faults developed at approximately right angles to the structure. These are primarily recognized at the surface by offsets in the Parkman Sandstone Member and by near-vertical calcite veins in some of the faults. These have been mapped and shown in plate 7 in Thom and Spieker (1931). McCutcheon (2003) has used these data and 3-D seismic data to determine the degree of extension of these faults into the subsurface, as well as their surface expression (Figure 5) (McCutcheon, 2003). This analysis was extended by M. Milliken (2003, personal communication) with aerial photography. A thorough study of the faulting in the Teapot Dome is important in the evaluation of its integrity as a CO_2 sequestration site.

The surface stratigraphy on the flanks of the Teapot Dome is dominated by the Parkman Sandstone Member of the Upper Cretaceous Mesaverde Formation (Figure 3). The Parkman Sandstone Member has been removed by erosion from the central part of the Teapot Dome, leaving the upper part of the Steele Shale at the surface. Extensive beds of bentonite in the Steele Shale undoubtedly control, to some extent, the hydrology of the area and serve as a seal on the shallow Shannon Sandstone Member, which is productive of hydrocarbons.

The Niobrara and Carlile shales underlie the Steele Shale. The Frontier Formation is hydrocarbon productive over the Powder River basin, as well as other basins in Wyoming. At Teapot Dome, three specific sandstones (First Wall Creek, Second Wall Creek, and Third Wall Creek) are recognized. The Second Wall Creek sandstone has been and continues to be the source for most of the oil production from the Teapot Dome (Figure 3). Both the Second Wall Creek and Shannon were significantly underpressured at the time of the baseline survey.

The Pennsylvanian Tensleep formation has two sandstone members, which are also hydrocarbon productive at Teapot, as well as elsewhere in Wyoming. Tensleep A and Tensleep B are relatively clean sands, producing petroleum and substantial low-salinity water (Figure 3). Below the Tensleep are other Paleozoic formations not penetrated by drilling, including the Mississippian Madison Limestone aquifer, which must not be used for sequestration experimentation.

METHODOLOGY

Sample Location, Measurement of Fluxes, Collection, and Measurement of Soil Gas

Previous flux measurements have demonstrated the spatial heterogeneity in both measured fluxes and in soil-gas concentrations. Each location was sampled in triplicate with three flux chambers (designated A, B, and C) set in a line 10 m (33 ft) apart. The flux chambers have a cross-sectional area of 1.00 m^2 (10.763 ft^2). The 1.00-m^2 (10.763-ft^2) flux chambers are at the upper limit of portability, but the large chamber areas have been demonstrated to reduce spatial variance. The flux chamber construction and operation were described in Klusman (2003a).

Forty locations on the Teapot Dome field and extending slightly off the field to the northeast were measured in January 2004 (Figure 6). Numbered stakes were placed at each location so that accurate recovery is

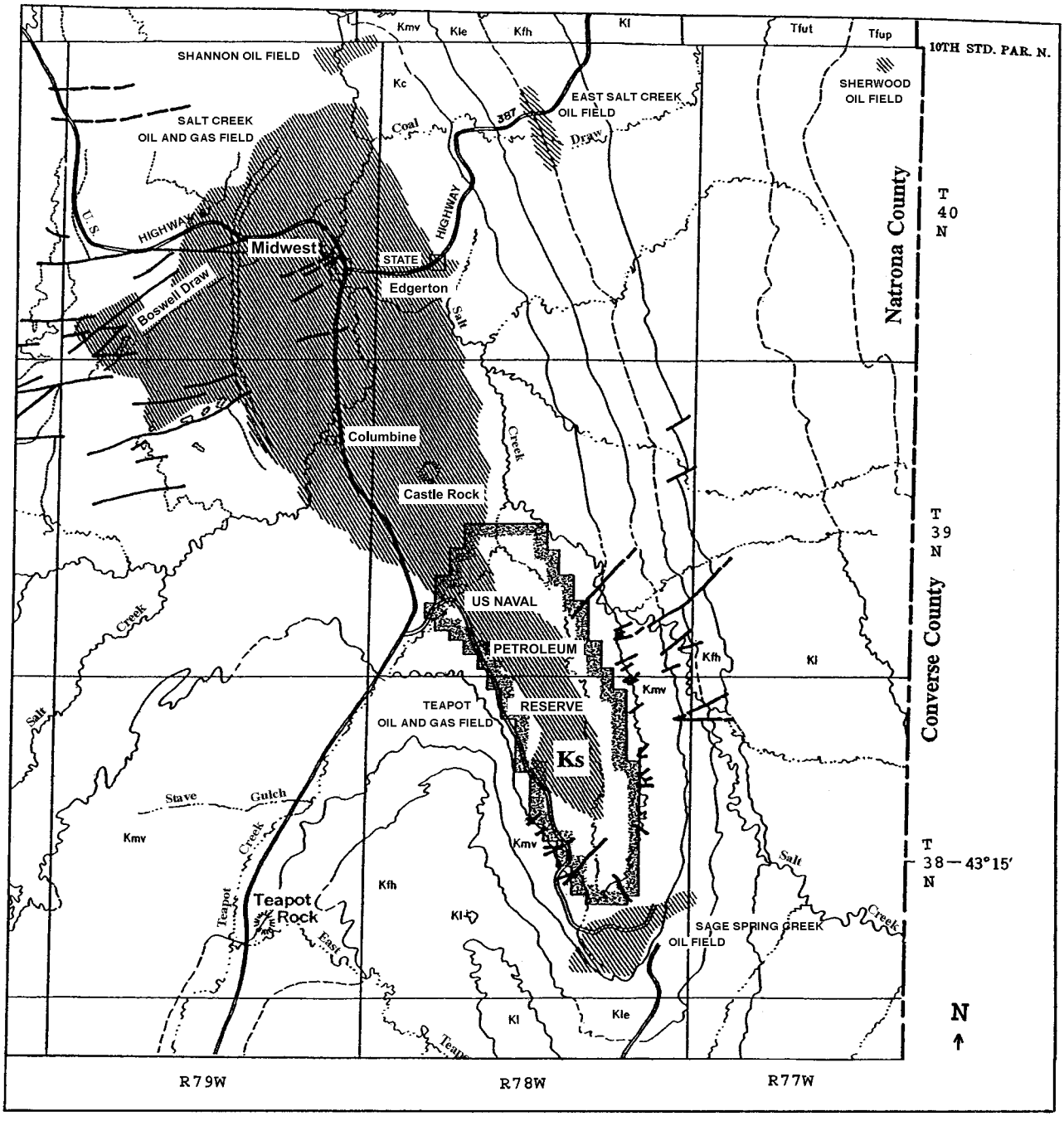

Figure 2. Plan view of the Teapot Dome oil field and the surrounding surface geology. Tfu = Fort Union Formation; Tfup = sandstone member forming Pine Ridge; Tfut = Tullock Member; Kl = Lance Formation; Kfh = Fox Hills Sandstone; Kle = Lewis Shale; Kmv = Mesaverde Formation; Ks = Steele Shale (Kc = Cody Shale in Weitz and Harbison, 1954); Kn = Niobrara Formation; Kf = Frontier Formation. The Castle Rock of Figure 2 is formed by the Shannon Sandstone Member in the middle of the Steele Shale (modified from Weitz and Harbison, 1954).

possible for subsequent measurements. The latitude–longitude of the locations was determined using a hand-held global positioning system unit and was for the A chamber or the B chamber for fault locations (Appendix). Compacted areas such as roads or well pads were avoided in the placement of the flux chambers. In general, sampling locations were selected to obtain a uniform coverage of the field.

Seven of the forty locations were specifically allocated to faults (Figure 6), primarily based on vein

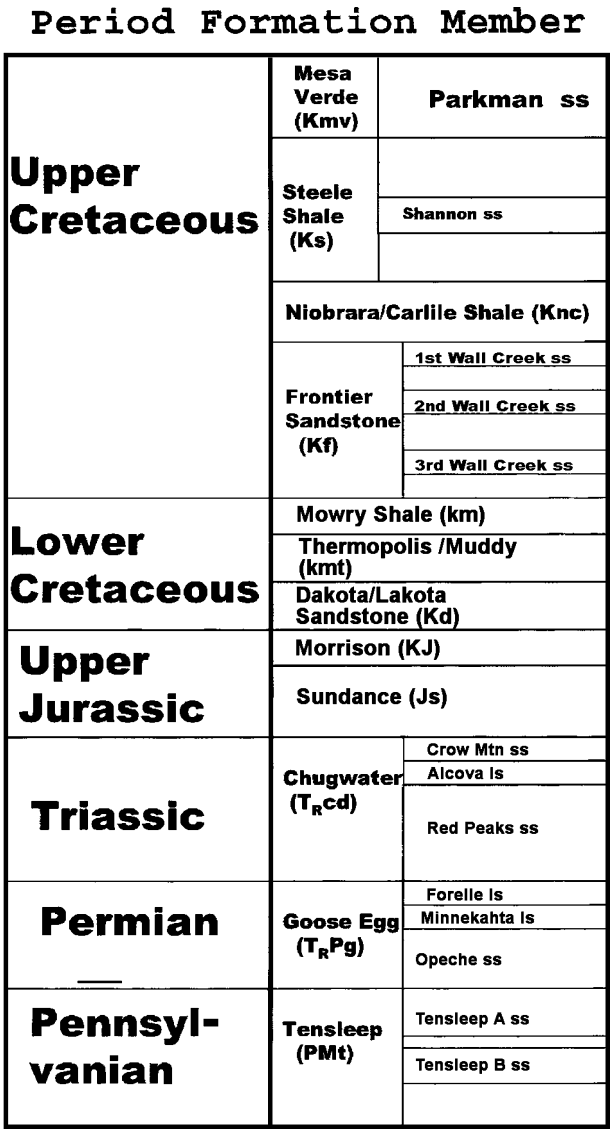

Figure 3. Stratigraphic section of the Teapot Dome oil field (modified from Thom and Spieker, 1931, plate 11; M. Milliken, 2004, personal communication). The Second Frontier in Figure 5 is equivalent to the Second Wall Creek of Figure 3.

calcite and soil alteration. These locations were in the S2 fault zone as defined by McCutcheon (2003). The individual splays of the S1 fault zone were more difficult to locate, so the precise placement of a chamber on a fault splay in the southern area was not possible. Locations 8, 9, 10, and 15 were in the S2 fault zone (fault T of Thom and Spieker, 1931) in Section 33, T39N, R78W. Locations 9 and 15 could be specifically located based on calcite veins, and locations 8 and 10 were based on projection. Locations 13 and 14 were in the northwest corner of Section 33 (fault S of Thom and Spieker, 1931). Location 13 is just east of a gully where vein calcite was visible, as well as a band of oxidized iron in the soil. Location 14 is immediately west of a gully where vein calcite was visible. Location 17 was placed just north of Conley Gulch in Section 3, T38N, R78W. This is in the southern part of the S2 fault zone (fault B1 of Thom and Spieker, 1931).

The 40 locations shown in Figure 6 were randomized and then sampled and measured in the random sequence. The randomization was specifically done so that no intraseasonal flux and soil-gas trends would appear in the data over the approximately 1 month of the field survey.

In this research, a real-time field measurement of CO_2 was made using a dual-channel, nondispersive Licor Model 7000 infrared instrument, which measured CO_2 and H_2O vapor. Details of this instrument and the measurement of CO_2 fluxes were described in Klusman (2003a, 2004).

Samples for CH_4 measurement and flux calculation were collected using a 25-mL gas-tight syringe and were taken at timed intervals from under the chambers through a septum in the side of the chamber. The details of the collection of CH_4 samples for flux determination and the collection of soil-gas samples were described in Klusman (2003a). The samples from flux chambers and soil gas were analyzed by the author using gas chromatography with flame ionization detection for CH_4 and thermal conductivity detection for CO_2 (Klusman, 2003a, 2004).

Carbon Isotopic Ratio Measurements on CO_2 and Various Solids

An important tool in the recognition of CO_2 and CH_4 from inorganic and biologic sources is stable carbon isotopy. The stable carbon isotopic ratio of materials is expressed using the equation

$$\delta^{13}C = \left[\frac{(^{13}C/^{12}C)_{sample}}{(^{13}C/^{12}C)_{standard}} - 1\right] \times 10^3 \qquad (1)$$

The units are parts per thousand (‰; per mil). Biological sources of carbon tend to be isotopically lighter (more negative or depleted) than inorganic sources. The determination of the probable source of a carbon-containing molecule can be aided by the use of stable isotopes.

The $\delta^{13}C$, relative to Peedee belemnite (PDB), for CO_2 was determined using isotope ratio mass

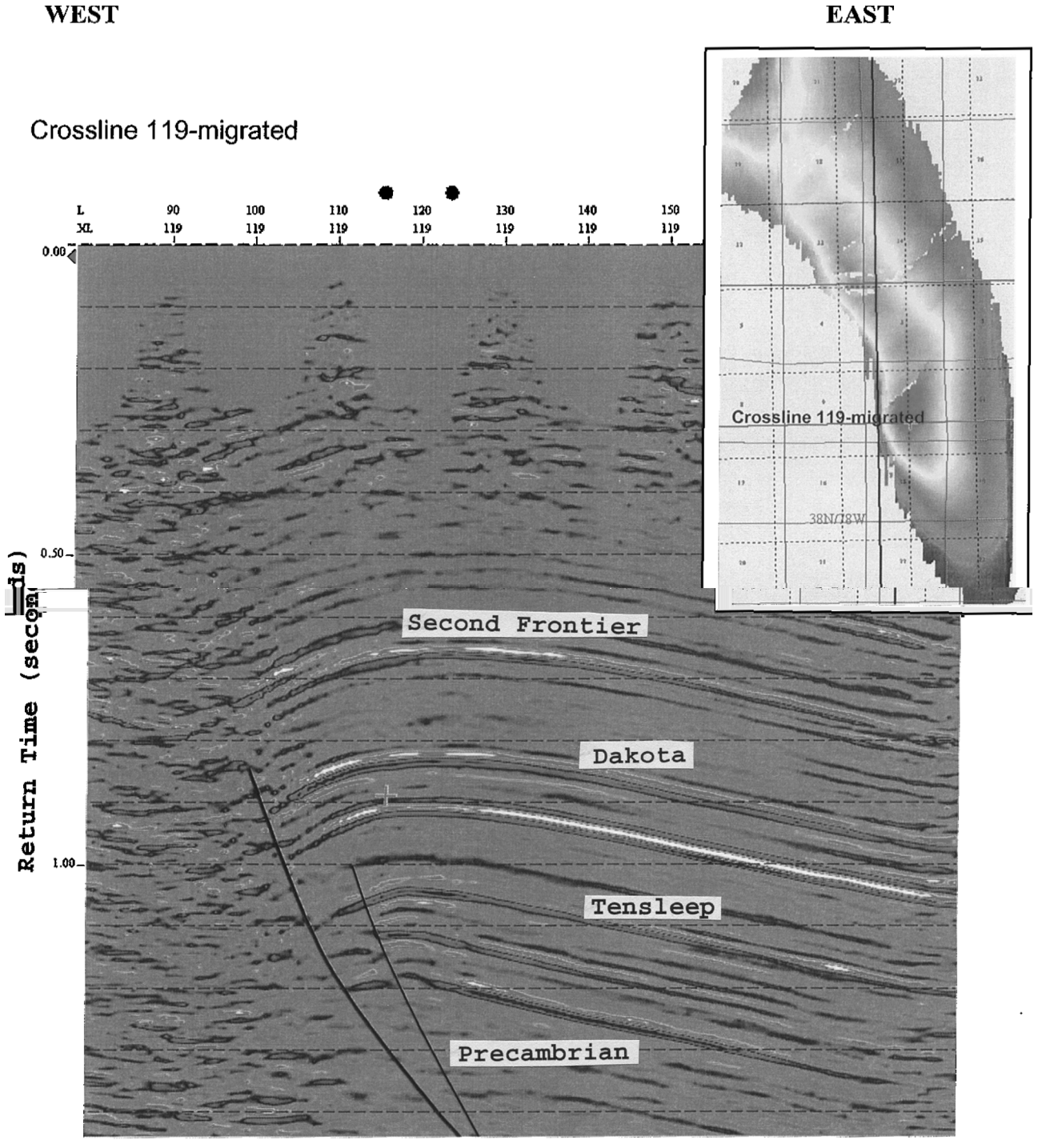

Figure 4. Plan view near 0 s traveltime and seismic cross section at crossline 119 illustrating the geometry of the Teapot Dome anticline (from McCutcheon, 2003).

spectrometry (IRMS) by Isotech Corporation of Champaign, Illinois. The PDB standard is the universal standard used for carbon in isotope geochemistry. Based on equation 1, the PDB standard has a defined value of 0.00‰.

Miscellaneous Samples and Measurements

During the course of the baseline soil-gas and gas flux measurements, one location was immediately recognized as anomalous, which was also on a fault (location 9,

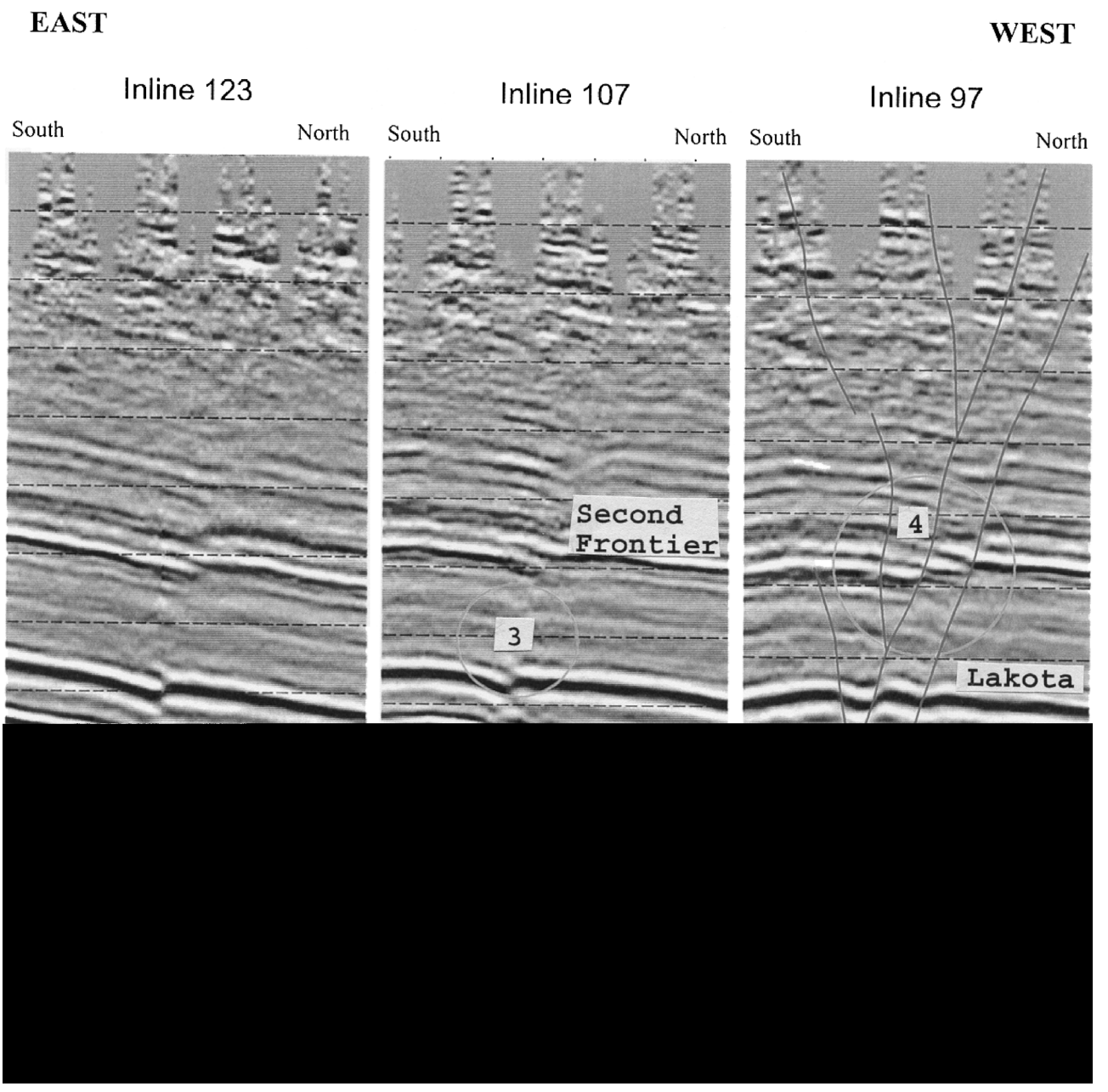

Figure 5. Seismic panels illustrating the geometry of the S2 dextral-oblique strike-slip fault zone. Points 1, 2, and 3 show vertical displacement of seismic horizons. Point 4 illustrates a negative flower structure (from McCutcheon, 2003).

Figure 6). A detailed sampling and analysis of CO_2 and CH_4 from soil gas over a 1.2-km (0.74-mi) length of the fault concluded that the anomalous location was caused by contamination.

Five 10-m (33-ft)-deep holes were drilled for future nested soil-gas measurements. The depth intervals for future measurements were 10, 5, 3, 2, and 1 m (33, 16, 10, 6, and 3 ft). During the drilling of the 10-m (33-ft)-deep holes at selected locations, bulk samples of drill cuttings were collected at the surface at 1, 2, 3, 5, and 10 m (3, 6, 10, 16, and 33 ft). The surface samples were soils, and the subsurface samples were upper Steele Shale in various stages of weathering, from highly weathered to nonweathered. Three determinations were made on these splits: $\delta^{13}C$ of the carbonate phase, $\delta^{13}C$ of the organic matter, and the organic matter content.

Type T thermocouples were buried at depths of 15, 30, 60, and 100 cm (6, 11, 23, and 39 in.) at each of four locations during October 2003. These were at

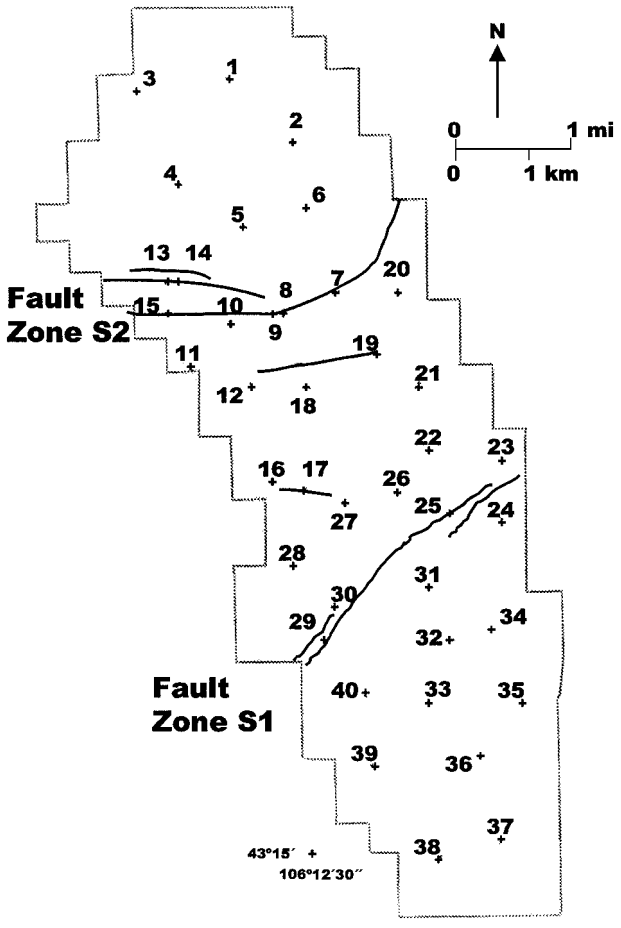

Figure 6. Sampling and measurement location map of the NPR-3, with fault zones S1 and S2 of McCutcheon (2003).

locations 7, 12, 24, and 32 (Figure 6). The temperature was measured at each of these depths and locations when visiting the NPR-3 field site to aid in future computer modeling of biological processes operating on soil gases.

Barometric pressure was recorded at hourly intervals in the motel room during baseline measurements of soil gas and gas fluxes.

Samples of vegetation, soil caliche, encrustations on alkali seeps, calcite vein material, and one ozokerite or soil wax sample were taken, and the author's breath was sampled for $\delta^{13}C$ determination. The carbon isotopic ratio determination of the author's breath is useful in assessing the possibility of CO_2 contamination of atmosphere samples. It is relatively difficult to manually sample the atmosphere for CO_2 without some risk of minor contamination.

During the drilling of the 10-m (33-ft) holes, very wet conditions were encountered during the drilling of the hole at location 19. By the next morning, the hole had filled with water up to a depth of approximately 8 m (26 ft). This water and a sample of water from a Tensleep well (72 TPX-10) were collected for standard oil-field determinations of major cations and anions.

Soil-gas permeability and porosity were determined during the summer of 2004. The soil-gas permeability was determined using a floating can gas permeameter (Evans, 1965) at four locations on the Teapot Dome field. This determination was made at approximately 15-cm (6-in.) depth intervals at each of the four locations, from the surface down to approximately 2 m (6 ft) depth. Two of these locations were in alluvial areas (location 2 and 21, Figure 6), and two were in higher elevation bedrock areas (locations 6 and northeast of 16, Figure 6).

RESULTS AND DISCUSSION

Surface Gas Flux Measurements

The flux and soil-gas measurements were carried out over the period of January 7–28, 2004. Figure 7a shows the distribution of CO_2 concentrations in air measured over this period. Figure 7b shows the probability distribution for the same data set, indicating a normal distribution. A probability distribution as shown in Figure 7b provides a more objective approach to assessing whether a histogram such as Figure 7a is a normal distribution. A normal distribution becomes a straight line in the probability plot. The mean and standard deviation were 379.0 and 2.98 ppmv, respectively.

The atmospheric CH_4 distribution and probability distribution are shown in Figure 8. The mean and standard deviation were 0.927 and 0.056 ppmv, respectively. The mean value is substantially less than the global atmospheric value. This could be caused by a calibration offset influenced by the low-concentration CH_4 standard or may be a natural variation. The Teapot Dome field is located at the southwest corner of the Powder River basin, upwind of the occurrence and production of coal and hydrocarbons. Cumulative methanotrophic oxidation of atmospheric CH_4 over a long upwind fetch may have resulted in some atmospheric depletion.

Figure 9 shows the distribution of CO_2 fluxes for the NPR-3 area. Figure 9a is the histogram, and Figure 9b is the probability distribution for 39 locations, excluding contaminated location 9. Figure 9b cleary shows that the linear fit to the data has been rotated by three locations at the high end (7, 18, and 26)

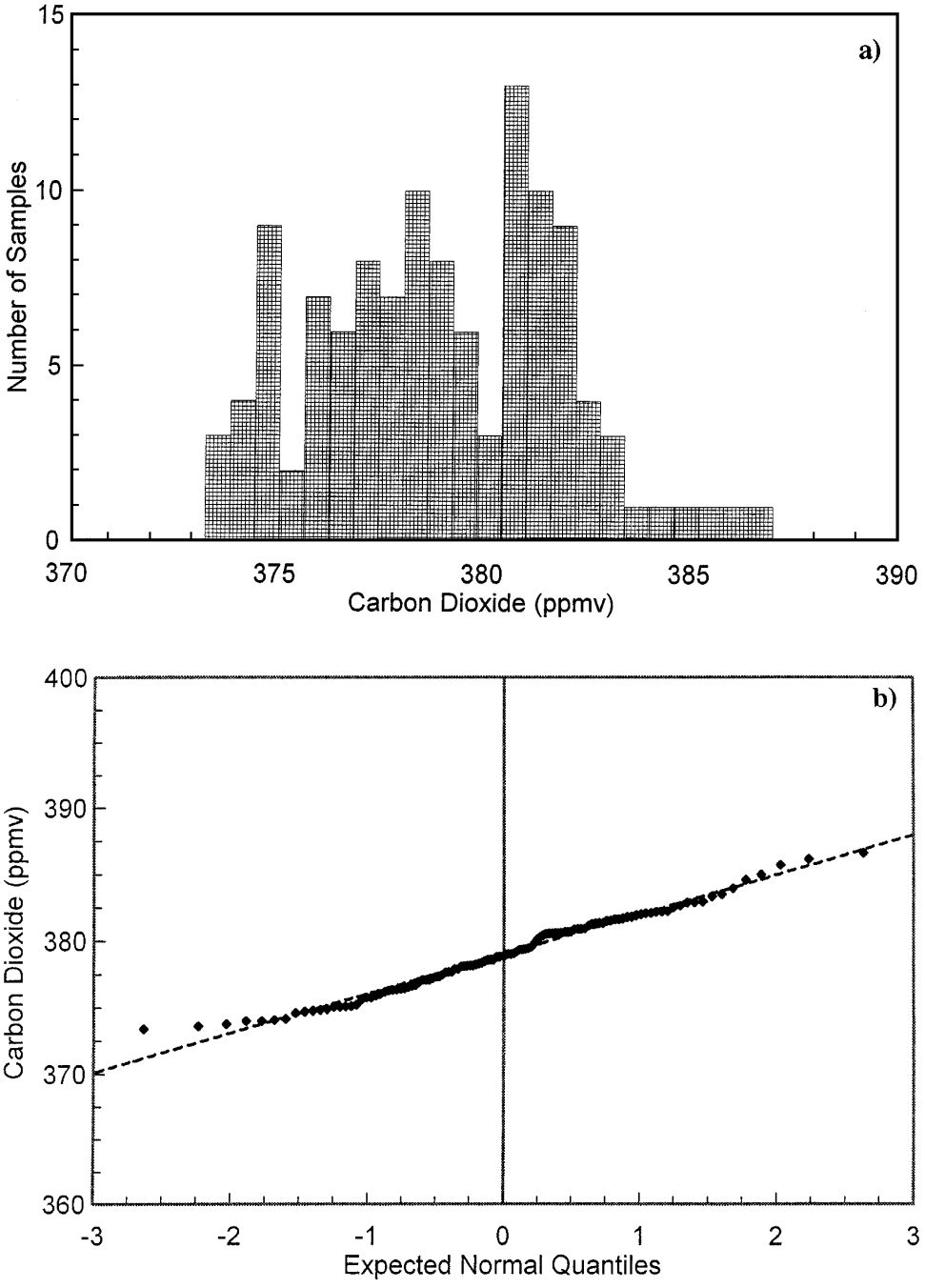

Figure 7. Distribution of atmospheric CO_2 during the NPR-3 baseline survey: (a) histogram and (b) probability diagram.

and one location at the low end (19). This can be used as a preliminary indication that these four locations were anomalous with respect to the remainder of the flux measurements. Only positive fluxes were expected, consistent with biological processes operating in the unsaturated zone, so that location 19, with a significant negative flux, has some other process operating. The removal of the four possibly anomalous samples leaves a distribution that is much closer to normal (Figure 9c).

Figure 10 is the geographic distribution of the CO_2 fluxes on an outline of NPR-3, corresponding to the locations in Figure 6. Variogram analysis suggested that there is a limited ability to contour the CO_2 flux data, so the data are posted as four percentile ranges in Figure 10. As predicted by variogram analysis, no obvious trends are apparent. Numeric data for gas fluxes and 100-cm (39-in.) soil gas for each location are in the Appendix.

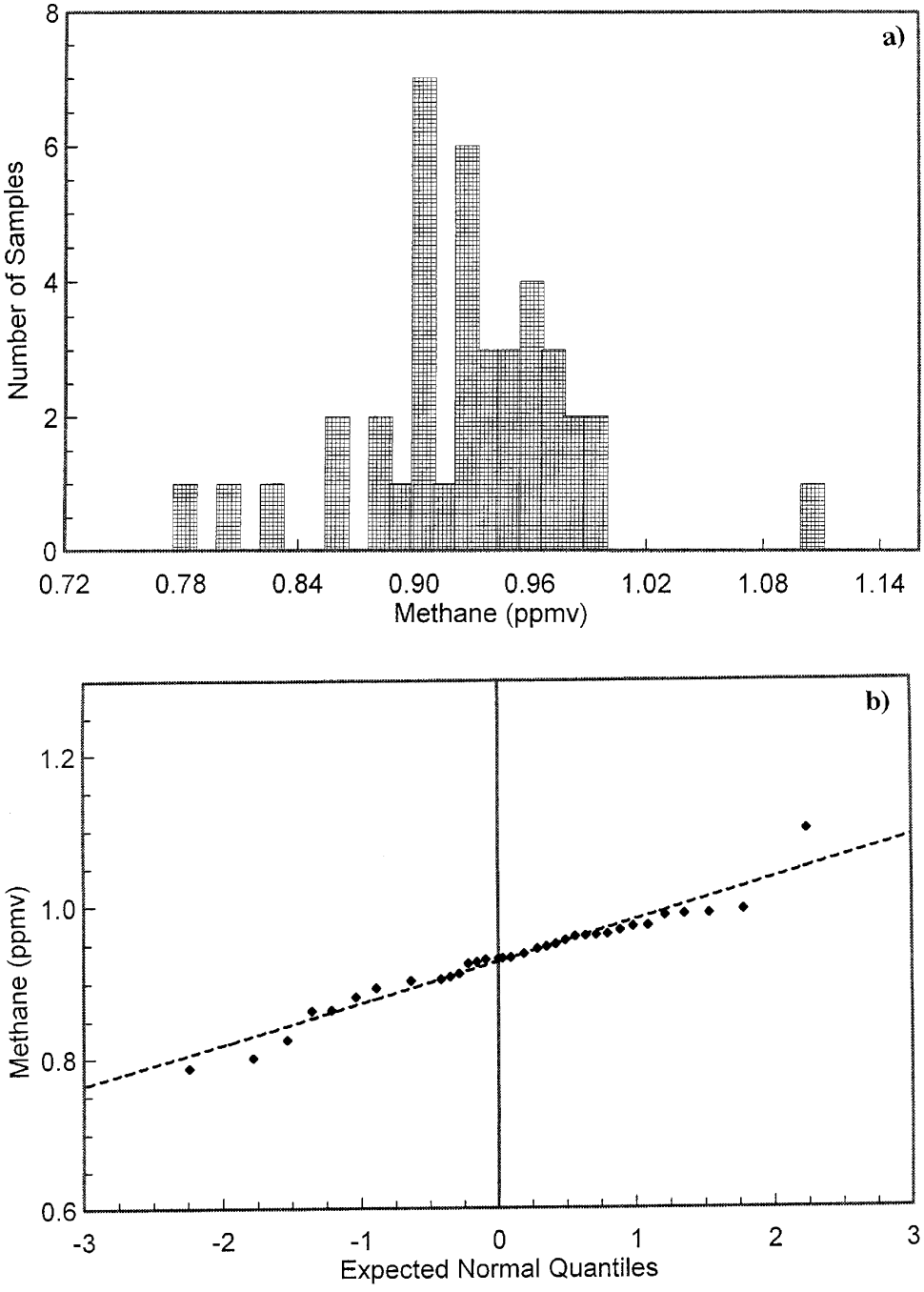

Figure 8. Distribution of atmospheric CH_4 during the NPR-3 baseline survey: (a) histogram and (b) probability diagram.

Figure 11 shows the distribution of CH_4 fluxes for the NPR-3 area. Figure 11a is the histogram, and Figure 11b is the probability distribution for 39 locations, excluding contaminated location 9. Figure 11a shows that CH_4 has both positive and negative fluxes, consistent with the prediction. In Figure 11b, it appears that there were two anomalous locations at the high end (5 and 33). This might be used as a preliminary indication that these two locations were anomalous with respect to the remainder of the CH_4 flux measurements.

Variogram analysis suggested that there is a limited ability to map the CH_4 flux data. The data are also posted as four percentile ranges in Figure 12. As predicted by the variogram analysis, no obvious trends are evident.

The flux data for CO_2 and CH_4 are summarized in Table 1. The similarity of the mean and the median

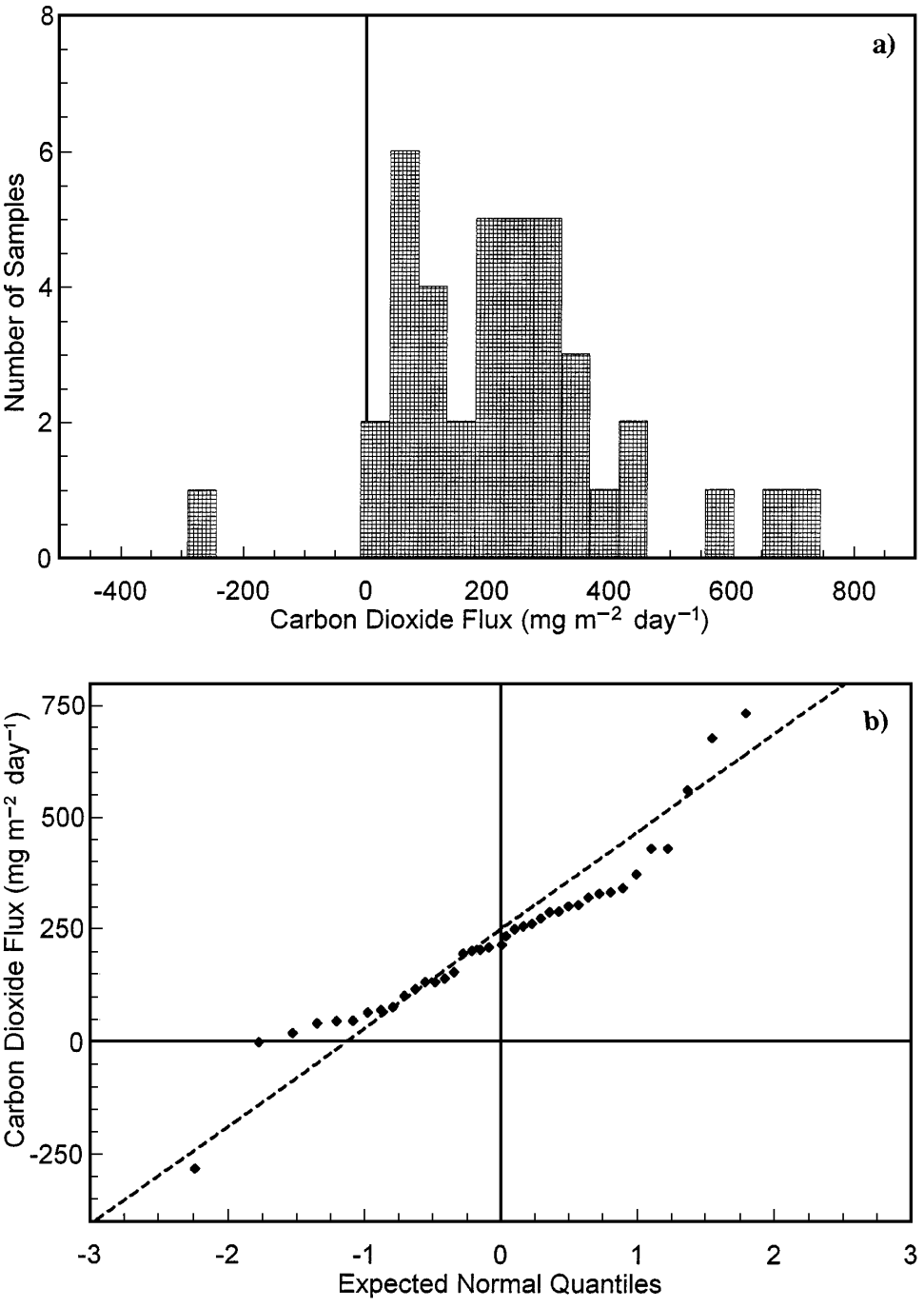

Figure 9. Distribution of CO_2 fluxes measured during the NPR-3 baseline survey: (a) histogram, (b) probability diagram, and (c) probability diagram with four anomalous locations removed.

reflects a near-normal distribution, in addition to Figures 9 and 11.

Table 2 summarizes the number of locations and chambers that fall into the categories of positive and negative fluxes. Commonly, this nonparametric tabulation is useful when the fluxes are so low, as is the case for CH_4. The distribution of CH_4 fluxes shown in Figure 11 can be further analyzed using the *t*-test. Table 3 illustrates this analysis and suggests that there was a small, positive CH_4 flux at the Teapot Dome.

The CO_2 and CH_4 fluxes at NPR-3 were compared to wintertime measurements at Rangely, Colorado. It must be recalled that Rangely has been operating a CO_2-EOR since 1986, and the reservoir is significantly overpressured. This contrasts with the underpressure in the Shannon and Second Wall Creek at Teapot at the time of the survey. Table 4 makes this comparison. The CO_2 at NPR-3 and Rangely have similar mean values, but the Rangely data show more variability, which was hypothesized to be caused by microseepage

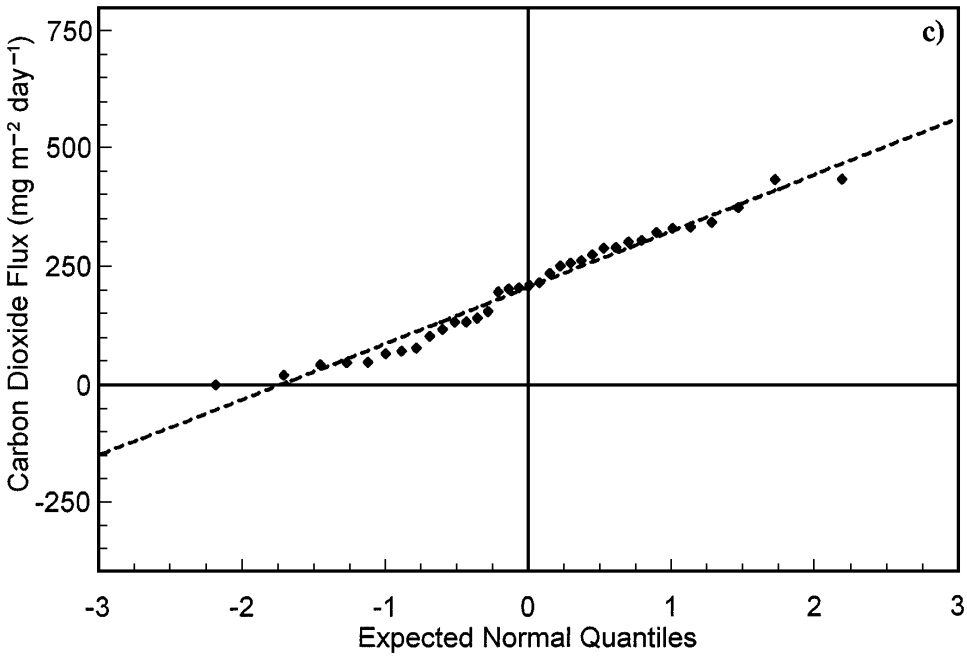

Figure 9. Continued.

of CH_4, which was then oxidized to CO_2 in the unsaturated zone (Klusman, 2003b). The mean CH_4 fluxes at Rangely were far higher than at NPR-3 and with greater variability. This also fits with the conclusion of measurable CH_4 microseepage at Rangely. The Shannon and Second Wall Creek reservoirs at Teapot are underpressured, which is consistent with a very low, negligible, or possibly undetected CH_4 flux to the surface shown in Table 1.

The data in Tables 1–4 can be put into context relative to the previously measured CH_4 fluxes in semiarid sedimentary basins of the western United States. In an earlier study on the potential for sedimentary basins to make a measurable contribution to the atmospheric CH_4 cycle, fluxes were measured in four basins where thermogenic production of hydrocarbons was occurring (Klusman et al., 2000). One of the basins was the Powder River basin, consisting of two east-west lines completely across the basin. The southern line passed just to the north of NPR-3. This earlier work demonstrated the importance of season in the evaluation of gas microseepage in a cold, dry climate.

Table 5 summarizes CH_4 flux data for 342 locations (1026 chambers) collected over a 3-yr period using the same chambers and methodology used in this study. The grand mean of all 1026 flux measurements was -0.12 mg CH_4 m^{-2} day^{-1}, with a standard error of 0.32. The median was -0.08 mg CH_4 m^{-2} day^{-1}. The 95% confidence limits about the mean were -1.13 to $+0.88$ mg CH_4 m^{-2} day^{-1}. There were 522 chambers with negative fluxes and 504 with positive fluxes. The median values for a particular data set are similar to the mean values, indicating near-normal distributions.

In general, Table 5 shows that lower (negative) CH_4 fluxes were measured in warmer months, and small positive fluxes were measured in cooler months. The standard deviation increased substantially in the spring measurements, reflecting increasing temperature and soil moisture, with rapid increases in biological activity. The data reflect seasonal rise and fall of methanotrophic activity superimposed on a relatively constant but low level of microseepage.

Soil-Gas Composition and Carbon Isotopic Measurements

Distribution data for soil-gas components will not be presented. Concentrations show the same degree of scatter as do the flux data for CO_2. Figure 13 is the 100-cm (39-in.) soil-gas CO_2 plotted as quartiles. Again, no particular pattern is apparent. Figure 14 contains the $\delta^{13}C$ for the 100-cm (39-in.) CO_2 plotted as quartiles. Table 6 summarizes the concentration data for CO_2 in soil gas. The 100-cm (39-in.) soil-gas CO_2 and CH_4 concentrations and $\delta^{13}C_{CO_2}$ are tabulated in the Appendix.

Figure 15 shows the soil-gas CH_4 at a depth of 100 cm (39 in.) as quartiles, and no pattern is apparent, consistent with variogram analysis. Table 6 summarizes concentration data for CH_4 in soil gas. Very

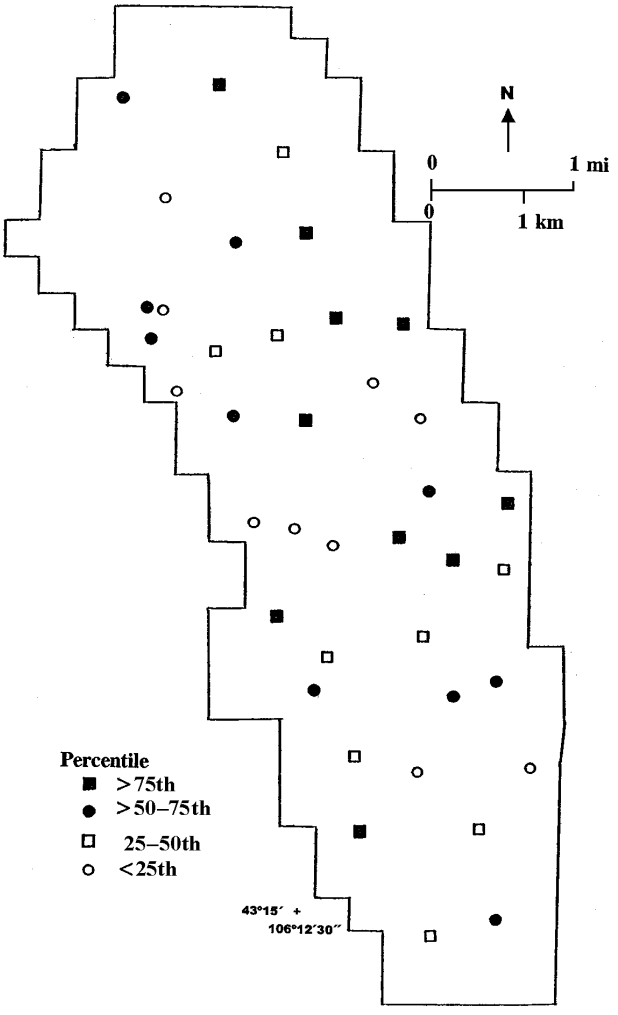

Figure 10. Carbon dioxide fluxes measured during the NPR-3 baseline survey posted as quartiles.

little variability with depth was also present, indicating that CH_4 was in a small background range, with very little evidence for the processes of microseepage or methanotrophy in the summary data.

A gas flux into the atmosphere is normally derived from a soil pore space in the case of a positive flux and from the atmosphere to the soil in the case of a negative flux. This should be reflected in the relationships between flux and soil-gas concentrations as shown in Table 7. Carbon dioxide flux correlated positively with concentration at all three measured depths, but only significantly at 100 cm (39 in.). Because the soils were frozen to a depth of approximately 60 cm (23 in.), most residual wintertime biological activity is at a depth below the frost line.

Figure 16 shows the mean and standard deviation for $\delta^{13}C$ in soil-gas CO_2 at all three depths and in the atmosphere for the 40 locations measured. The carbon isotopic shift is in the direction indicating a predominance of a carbon-13 depleted, biologically derived CO_2 in the soil gas. The magnitude of the carbon isotopic shift and soil-gas CO_2 concentrations correlate significantly, indicating a predominance of the biological source for soil-gas CO_2.

Another way to view the isotopic shift for gases is with a plot as shown in Figure 17. This approach works for gaseous end members but cannot accommodate organic solids from which a gas such as CO_2 may be derived. Figure 17 is a plot of the $\delta^{13}C$ value of CO_2 plotted vs. $\ln(1/CO_2)$, which linearizes the relationship. The measured atmospheric CO_2 concentrations and the vegetation with the organic fraction from 10-m (33-ft) hole cuttings serve as pure end members. The line represents simple physical mixing of various proportions of end members, with no chemical or biological modification.

The 100-cm (39-in.) soil-gas CO_2 from 39 locations (excluding location 9) fall between the two end members. The bulk of the measurements fall below the line connecting them, most likely because of isotopic fractionation during biological decay of organic matter, favoring production of CO_2 that is isotopically lighter than the organic substrate from which it is primarily derived. The water (and gaseous CO_2 in equilibrium with the water) from Tensleep well 72 TPX-10 is the single point in the upper left corner of Figure 17, with a $\delta^{13}C$ value of +0.06‰. Figure 17 shows where dissolved CO_2, or gaseous CO_2 in the Tensleep Sandstone, may fall as a pure geologic end member. Location 18 is an outlier, both with respect to concentration and stable carbon isotopic ratio. This was interpreted as an indication of microseepage and possibly methanotrophic oxidation of reservoir CH_4 to CO_2 in the shallow, unsaturated zone.

Location 18 was not a simple mixture of atmospheric CO_2 and CO_2 from organic decay. The source of the CH_4 was not necessarily the Tensleep Sandstone but may be a reservoir higher in the section. However, location 18 clearly had a geologic component.

The CH_4 flux and soil-gas concentrations correlated negatively at all three depths in Table 7, consistent with methanotrophic oxidation, which is more significant below the frost line. Even with this, there was a small net positive CH_4 flux, suggesting the possibility of a very low rate of CH_4 microseepage. The correlations among soil-gas CO_2 and soil-gas CH_4 at all three depths was very low and not significant.

Table 8 makes the comparison between soil-gas concentrations at NPR-3 and at Rangely, Colorado,

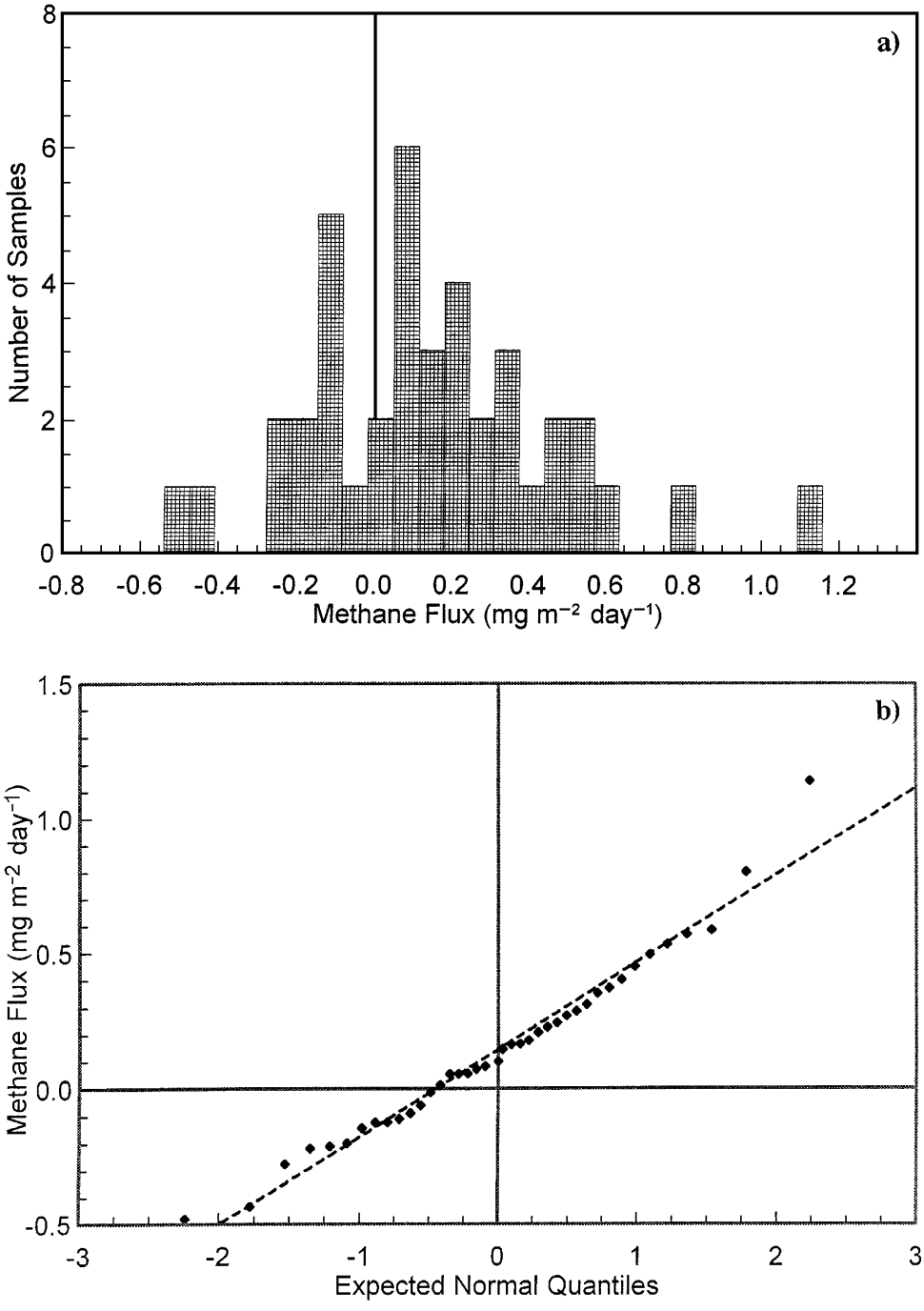

Figure 11. Distribution of CH_4 fluxes measured during the NPR-3 baseline survey: (a) histogram and (b) probability diagram.

which has undergone CO_2-EOR since 1986. CO_2 concentrations were clearly similar and were part of the evidence, along with isotopic data, that CO_2 microseepage was not occurring at Rangely. The situation for CH_4 is different. Mean values for CH_4 in soil gas were much higher at Rangely, with the highest being at a relatively small number of locations. This, along with isotopic evidence, suggested that CH_4 microseepage was occurring at Rangely. The NPR-3 data suggest very little or no microseepage of either CO_2 or CH_4, with the possible exception of a few locations. The wintertime measurements have captured the baseline conditions at Teapot Dome.

Stable Carbon Isotopic Ratios for CO_2 and Other Materials at Teapot Dome

Table 9 summarizes the carbon isotopic composition of materials that may influence the isotopic ratios in shallow and deep soil gas and in flux samples. It is in

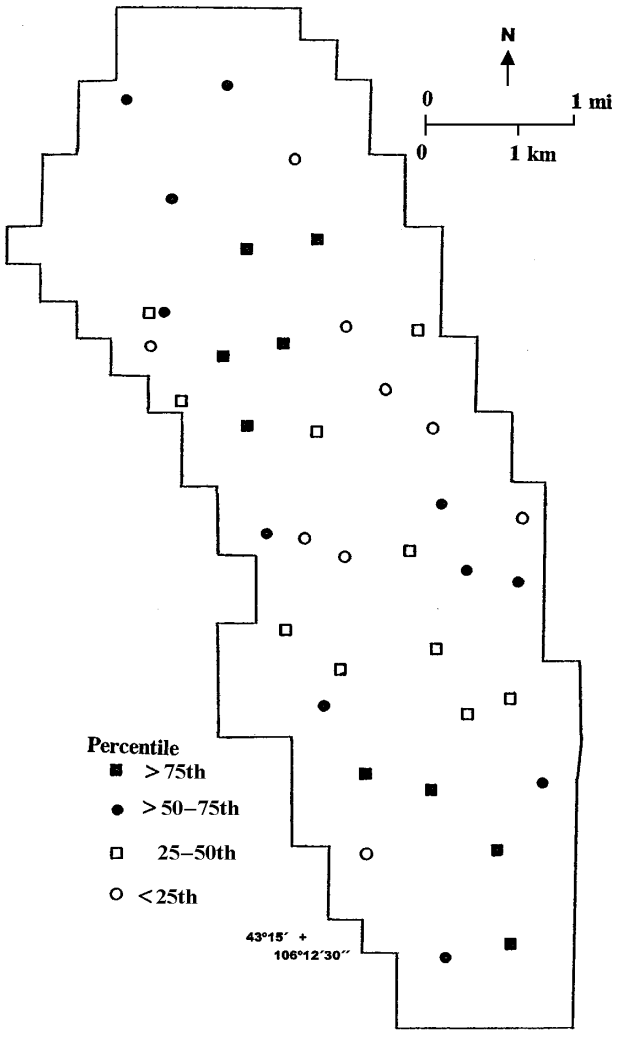

Figure 12. Methane fluxes measured during the NPR-3 baseline survey posted as quartiles.

the context of the data in Table 9 that interpretations as to the possible source of a carbon-containing gas must be made. The error in an individual $\delta^{13}C$ determination is from ±0.2 to ±0.3‰.

Because an objective is to determine if there was microseepage of hydrocarbons from a deep source, a determination was made whether any calcite, excluding caliche, found on the surface might be derived from microseeping hydrocarbons. Inorganic calcite formed in the marine environment typically has a $\delta^{13}C$ near 0‰. Cuttings from the 10-m (33-ft) holes penetrating the Steele Shale had a $\delta^{13}C$ for the carbonate phase of -1.10 ± 1.02‰. Excluding two of the isotopically lightest from the 30 samples for reasons related to possible microseepage in two of the 10-m (33-ft) holes increased the $\delta^{13}C$ for the carbonate phase to -0.88 ± 0.59‰.

Caliche is formed by the evaporation of water from soil pores, which contain dissolved bicarbonate ion, which, in turn, is derived from the dissolution of atmospheric CO_2 in precipitation (meteoric water). Isotopic fractionation is present in these reactions, resulting in caliche whose $\delta^{3}C$ value is heavier or more enriched than that of atmospheric CO_2. When measuring soil-gas CO_2, it is important to avoid seasons when caliche is actively dissolving and/or precipitating (late winter to late spring). Measurements of CO_2 in soil gas during this period tend to be variable and inconsistent, in part because of this process. As shown in Table 9, a value of -1.95 ± 0.26‰ was determined for caliche in soils at Teapot.

A sample of residual paraffin (ozokerite or soil wax) collected near location 17 had a $\delta^{13}C$ value of −30.4‰, and a δD of −143‰, which is a reasonable value for a weathered, devolatized petroleum residue. If there was hydrocarbon seepage along faults or fractures, with

Table 2. Nonparametric Summary of Microseepage

	Positive Flux	Negative Flux
CO_2 flux by location	38	2
CO_2 flux by chamber*	107	9
CH_4 flux by location	27	13
CH_4 flux by chamber*	75	45

*Three chambers per location.

Table 1. Summary Flux Data for the NPR-3 Baseline Survey (mg m^{-2} day^{-1})*

	Mean	Median	Standard Deviation	Range
CO_2 flux	227.1	214.1	186.9	−281.7 to 732.9
CH_4 flux	0.137	0.102	0.326	−0.481 to 1.139

*Not including contaminated location 9.

Table 3. Methane Microseepage Relative to Zero*

Mean = 0.137 mg m^{-2} day^{-1}
One sample *t*-test compared to zero. $t = 2.65$; two-tailed probability = 0.0091
Mean = 0.035–0.240 mg m^{-2} day^{-1} at 95% confidence
Mean = 0.0017–0.273 mg m^{-2} day^{-1} at 99% confidence

*Calculated by chamber.

Table 4. Comparison of Fluxes at NPR-3 and Rangely (mg m^{-2} day^{-1})

		Mean	Median	Standard Deviation
NPR-3	CO_2	227.9	214.1	186.9
	CH_4	0.137	0.102	0.326
Rangely	CO_2	302.0	67.9	1134
	CH_4	25.1	0.875	135

subsequent partial oxidation in circulating meteoric water, the $\delta^{13}C$ of any $CaCO_3$ formed should be intermediate between that of caliche and the seeping hydrocarbons. The isotopic shift may be an estimate of the proportion of carbon from each of the two sources.

Four samples of each of the four species of vegetation common on NPR-3 were collected for the determination of carbon isotopic ratio: big sagebrush, rabbit brush, western wheat grass, and blue gramma grass (Table 9). All four of these plants are C3-type species, using the Calvin-Benson photosynthetic cycle, and had an average $\delta^{13}C$ value of $-25.69 \pm 2.59‰$. Whether there were interspecies differences in Table 9 is not clear, but is not important for purposes of interpretation. More than four species of plants are present on NPR-3, and the soil organic matter is an unknown composite of all of them.

The average $\delta^{13}C$ of the organic fraction from soils and cuttings from the 10-m (33-ft) holes was $-25.94 \pm 1.16‰$ (Table 9). The degree of carbon isotopic fractionation that may occur during plant decomposition is unknown. Finally, the stable carbon isotopic ratio in CO_2 from the sampler's breath was $-22.92 \pm 0.42‰$. This indicated a diet of both C3- and C4-derived plants (or animals consuming these plants),

Table 5. Measured CH_4 Flux Values in the Sedimentary Basins where Thermogenic Microseepage may be Expected (mg $m^{-2}day^{-1}$)*

Date	*N***	Mean	Median	Standard Deviation
Denver-Julesburg				
September 1994	28	0.95	0.67	2.10
February–March 1995	28	0.46	−0.14	6.20
September 1995	28	0.29	0.78	3.89
Railroad Valley				
May 1995	60	−0.45	−0.065	2.47
July 1996	60	0.02	−0.001	1.45
Powder River				
November 1994	26	0.72	0.85	3.07
March 1995	26	−0.01	−1.30	6.23
August 1995	26	−0.64	−0.12	1.84
Piceance				
July 1995	30	−1.87	−2.24	2.08
August 1996	30	−0.029	−0.017	0.154

*From Klusman et al. (2000), modified by permission of the American Geophysical Union.

***N* is the number of locations where triplicate flux measurements were made during each season. The successive seasonal measurements were made at exactly the same locations.

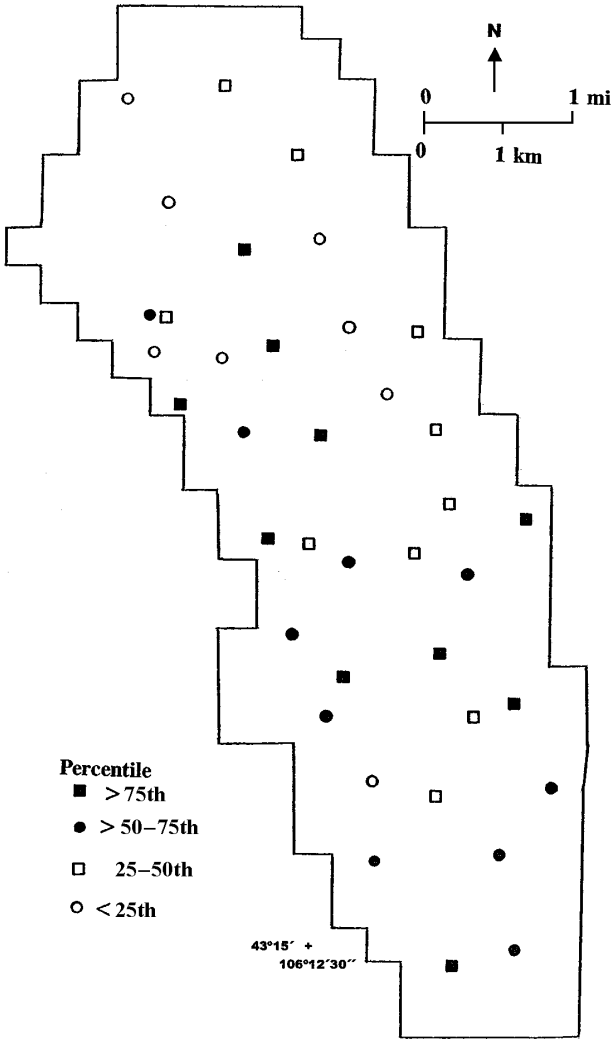

Figure 13. The 100-cm (39-in.) soil-gas CO_2 measured during the NPR-3 baseline survey as quartiles.

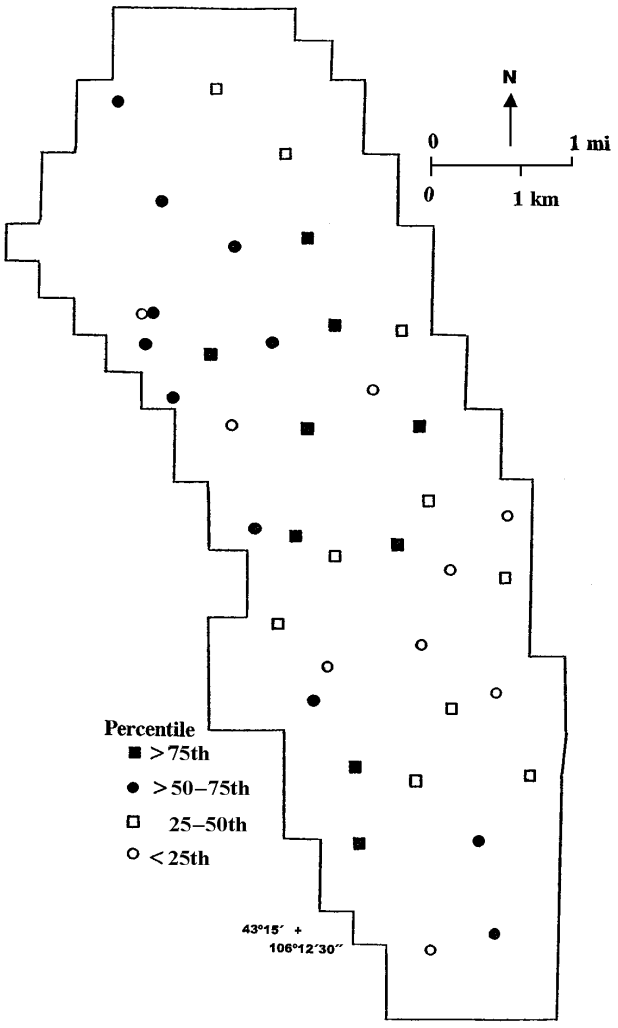

Figure 14. $\delta^{13}C$ of 100-cm (39-in.) soil-gas CO_2 measured during the NPR-3 baseline survey as quartiles.

with a predominance of C3 sources. This is relevant in the sampling and measurement of atmospheric CO_2.

Alkali seeps are relatively common at NPR-3. These are fragile, soft, white encrustations that occur both associated with faults and associated with scattered bentonite beds in the Steele Shale. The encrustations occur on the surface of soils and as coatings on dead vegetation. Samples from four locations were taken for x-ray diffraction analysis and for $\delta^{13}C$ determination on any minor carbonate minerals that might be present. The encrustations have a slightly bitter taste, suggesting the possibility of epsomite, $MgSO_4 \cdot 7H_2O$. The material is also almost instantly soluble in water. Table 9 contains the $\delta^{13}C$ value for three of the samples, suggesting what minor carbonate is present is derived from crystallization from water with a meteoric source. The fourth was contaminated with some decomposed vegetative material, which caused a significant isotopic shift to a lighter value.

The x-ray diffraction analysis showed a predominance of the sparse evaporite mineral konyaite, $Na_2Mg(SO_4)_2 \cdot 5H_2O$, thenardite, Na_2SO_4, and gypsum, $CaSO_4 \cdot 2H_2O$. Occasional quartz and K-feldspar were noted, indicating some inclusion of material from the Steele Shale. The konyaite would result in a slight bitter taste, but not as strong as the expected epsomite. Weathered, corroded crystals of gypsum are commonly found on the surface in areas of bentonite. A possible relationship of the alkali seeps to microseepage of reservoir fluids seems unlikely.

The simplest approach to using the data of Table 9 in the interpretation of soil-gas and flux data is to determine the isotopic shift from the atmospheric value (Figure 18). A unique solution to the proportion(s) of any of the three end members is not easy without additional measurements. A shift in either direction will indicate a predominant source for CO_2.

Placing some of the data from Table 9 on an isotopic shift diagram gives Figure 18. The soil-gas data in Table 9 indicate a predominance of a biological source for the samples at all three sampled depths, even in the winter. The vegetation and the organic fraction from the 10-m (33-ft) hole cuttings also show the biological

Table 6. Summary Concentration and Isotope Data for CO_2 and CH_4 in Soil Gas (ppmv)*

Depth (cm)	Mean	Median	Standard Deviation	Range
CO_2				
30	618	548	284	383–1944
60	645	590	199	373–1086
100	1010	719	1194	393–7783
$\delta^{13}C$ for CO_2 (‰)				
30	−16.02	−15.40	2.58	−26.9 to −11.6
60	−16.22	−16.40	1.94	−20.7 to −12.7
100	−15.29	−15.80	2.24	−19.7 to −9.0
CH_4				
30	0.940	0.960	0.128	0.660–1.535
60	0.919	0.935	0.114	0.506–1.216
100	0.923	0.956	0.093	0.627–1.102

*Not including contaminated location 9.

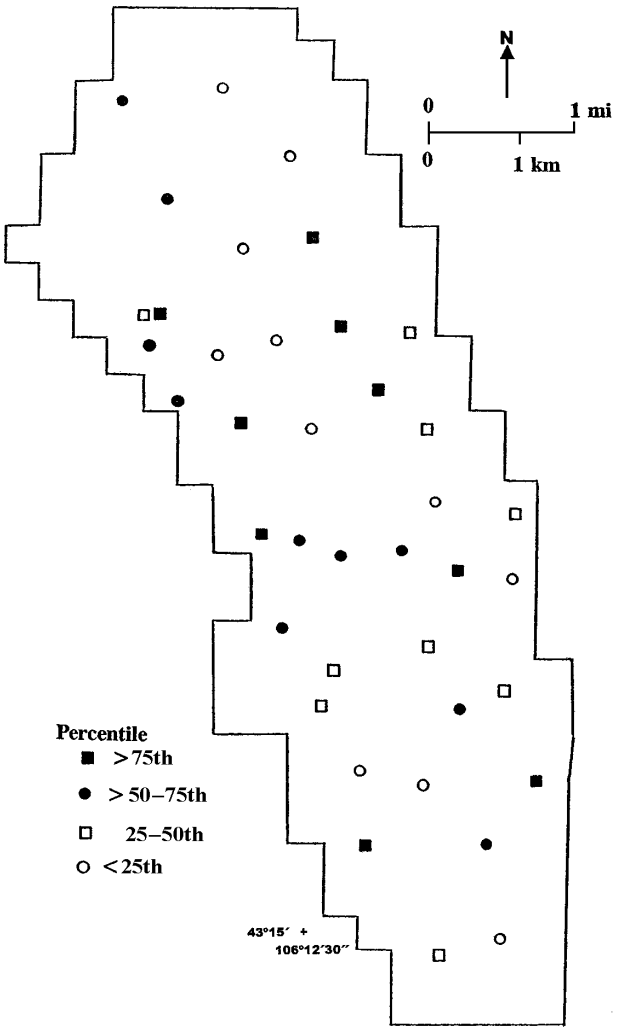

Figure 15. The 100-cm (39-in.) soil-gas CH_4 measured during the NPR-3 baseline survey as quartiles.

domination and primarily of the C3 photosynthetic pathway. The author's breath is obviously an organic source, but with a small shift in the direction of a contribution from a C4 photosynthetic pathway. The single sample of ozokerite (soil wax) is reasonable for a weathered petroleum residue but otherwise is not directly related to other samples in Figure 18.

The inorganic fraction of the 10-m (33-ft) hole cuttings, the minor carbonate in the alkali seeps, and the caliche show carbon isotopic characteristics of a purely inorganic process. This is probably the crystallization of $CaCO_3$ from atmospheric CO_2 dissolved in meteoric water.

The vein calcite from the fault zone S2 and the silky calcite from the same area show a shift from the purely inorganic contribution, suggesting a partial contribution of a microseepage source of hydrocarbons. The hydrocarbons are oxidized and mixed with the meteoric source of CO_2 to produce $CaCO_3$. The silky calcite was of a different textural phase that may have had a different origin than S2 calcite, but the carbon isotopes suggested it is genetically related to the S2 calcite. The vein calcite from the vicinity of location 17 shows a smaller shift, suggesting a smaller contribution of oxidizing hydrocarbons relative to CO_2 dissolved in meteoric water.

SUMMARY AND CONCLUSIONS

Baseline measurements of CO_2 and CH_4 fluxes into the atmosphere and shallow soil-gas concentrations were determined at the Teapot Dome oil field in NPR-3, in Natrona County, Wyoming. The bulk of these measurements were carried out in January 2004, when the noise caused by biological activity in the soils was at a minimum. The data are to provide a baseline for comparison with future measurements after CO_2 injection experiments have been in operation and may have perturbed the baseline condition.

A major concern in the expansion of CO_2 sequestration is the potential for gas leakage by processes of microseepage or migration up faults and fractures. Methane is as much of a concern as CO_2 because of its mobility in the subsurface and the potential for migration under the overpressure necessary for CO_2 injection at appreciable rates. A baseline characterization is important at Teapot Dome and should be a part of all fields proposed for CO_2-EOR, particularly if they are to be gradually shifted to a sequestration operation.

Carbon dioxide fluxes were determined by a field-portable infrared spectroscopic method using 1.00-m^2 (10.763-ft^2) chambers, in triplicate, at each of the

Table 7. Correlations among Gas Fluxes and Soil Gas Concentrations

	CO_2	CH_4
Flux and 30 cm (11 in.) soil gas	0.151	−0.273
Flux and 60 cm (23 in.) soil gas	0.231	−0.069
Flux and 100 cm (39 in.) soil gas	0.446*	−0.381**

*Significant at $\alpha = 0.01$.
**Significant at $\alpha = 0.05$.

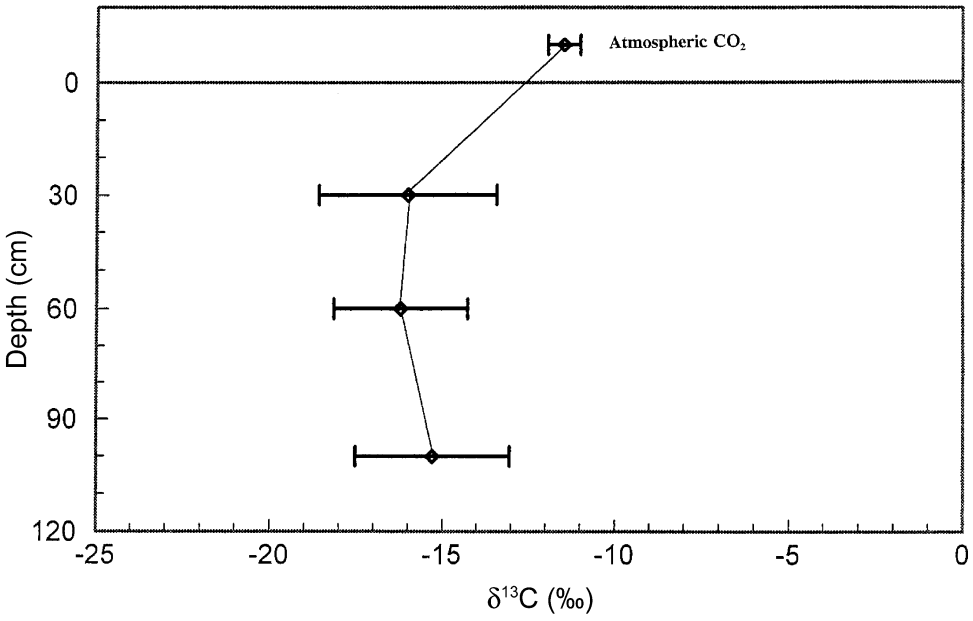

Figure 16. Carbon isotopic shift of CO_2 in soil gas at NPR-3. The central point is the mean, and the error bars are ±1 standard deviation.

40 locations on the field. Methane fluxes were determined under the same chambers by taking discrete samples, and the determination of the CH_4 was done by gas chromatography with flame ionization detection. Soil-gas CO_2 and CH_4 were sampled at 30-, 60-, and 100-cm (11-, 23-, and 39-in.) depths at each of the 40 locations using a soil-gas probe. Gas concentrations were determined by gas chromatography, using either flame ionization detection or thermal conductivity detection and methanized CO_2.

Carbon dioxide fluxes averaged 227.1 mg CO_2 m^{-2} day^{-1}, a standard deviation of 186.9 mg m^{-2} day^{-1}, and a range of −281.7 to 732.9 mg m^{-2} day^{-1}, not including contaminated location 9 with near-surface infrastructure contamination. Methane fluxes averaged 0.137 mg CH_4 m^{-2} day^{-1}, standard deviation of 0.326 mg m^{-2} day^{-1}, and a range of −0.481 to 1.14 mg m^{-2} day^{-1}, not including location 9.

Soil-gas CO_2 concentrations increased with depth, averaging 618, 645, and 1010 ppmv at 30, 60, and 100 cm

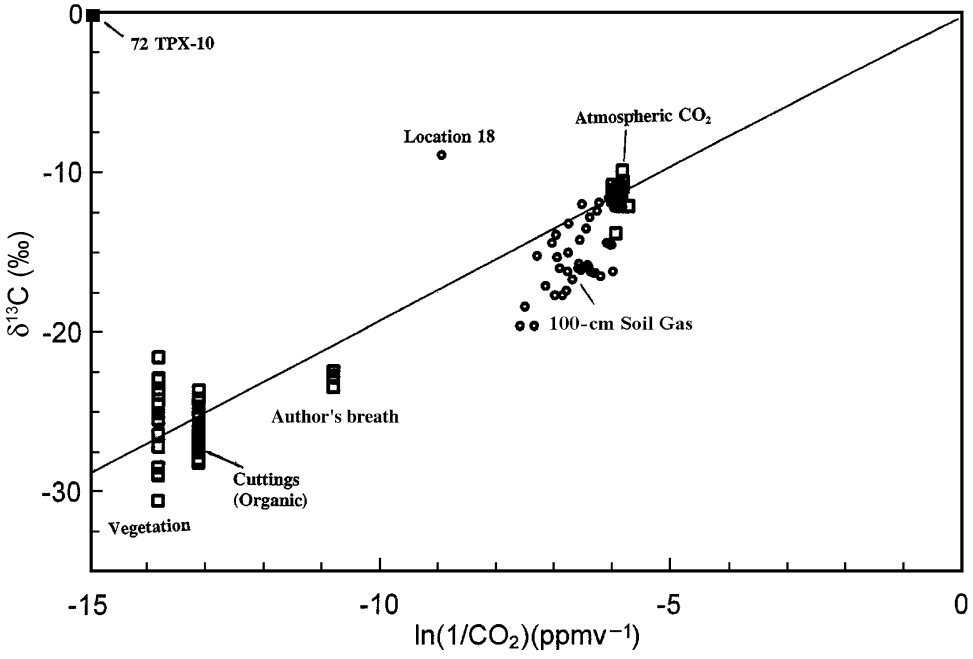

Figure 17. $\ln(1/CO_2)$ vs. $\delta^{13}C$ of CO_2 plot for atmospheric and biological end members and for the 100-cm (39-in.) soil gas.

Table 8. Comparison of Soil Gases at NPR-3 and Rangely (ppmv)

	Mean	Median	Standard Deviation
NPR-3 CO_2			
30 cm (11 in.)	618	547	284
60 cm (23 in.)	645	590	199
100 cm (39 in.)	1010	874	1194
Rangely CO_2			
30 cm (11 in.)	680	541	449
60 cm (23 in.)	865	542	1240
100 cm (39 in.)	1023	596	1260
NPR-3 CH_4			
30 cm (11 in.)	0.940	0.960	0.128
60 cm (23 in.)	0.919	0.935	0.114
100 cm (39 in.)	0.923	0.956	0.093
Rangely CH_4			
30 cm (11 in.)	1547	2.93	9603
60 cm (23 in.)	1581	2.93	9737
100 cm (39 in.)	3628	2.98	18867

(11, 23, and 39 in.), respectively. Soil-gas CH_4 concentrations averaged 0.128, 0.114, and 0.093 ppmv at 30, 60, and 100 cm (11, 23, and 39 in.), respectively. The decrease in CH_4 with depth reflects a slow rate of methanotrophic oxidation, even during winter conditions. The $\delta^{13}C$ of the soil-gas CO_2 was also determined in the soil-gas samples and in the atmosphere. These data demonstrated that the increased CO_2 with depth was derived from the biological oxidation of soil organic matter.

A variety of materials on the surface were characterized with respect to stable carbon isotopic ratios. These materials include vein calcite associated with faults and fractures, silky calcite, soil caliche, vegetation, alkali seeps, one sample of soil wax (ozokerite), and the inorganic and organic fraction of the cuttings from 10-m (33-ft) holes. The vein calcite in faults showed some isotopic shift, suggesting a mixture of meteoric water and lesser amounts of CO_2 from oxidized hydrocarbons, forming the calcite.

The data from the 40 locations were used to select 5 locations for more detailed measurements and for future study of processes operating in the shallow, unsaturated zone. Holes 10 m (33 ft) deep were drilled at five locations. These were equipped to allow future sampling of larger volumes of gas at depths of 10, 5, 3, 2, and 1 m (33, 16, 10, 6, and 3 ft)

Table 9. Carbon Isotopic Composition of Various Materials Sampled

	n	Average $\delta^{13}C$	Standard Deviation
Atmospheric CO_2 January 6–28, 2004	39*	−11.48	0.47
Klusman Breath	4	−22.92	0.42
Calcite Vein Material (all)	6	−7.97	3.96
S2 fault zone	4	−10.15	2.44
Location 17	2	−3.60	1.84
Silky calcite	3	−10.22	0.38
Soil Caliche	4	−1.95	0.26
Vegetation (all)	16	−25.69	2.59
Big sagebrush	4	−26.68	1.63
Rabbit brush	4	−23.02	1.02
Western wheat grass	4	−28.10	2.91
Blue gramma grass	4	−24.98	1.49
Alkali Seeps	3**	−1.30	1.74
Soil Cuttings from 10-m (33-ft) Holes			
Inorganic fraction	30	−1.10	1.02
Organic fraction	30	−25.94	1.16
Soil Gas			
30 cm (11 in.)	39†	−16.02	2.58
60 cm (23 in.)	39†	−16.22	1.94
100 cm (39 in.)	39†	−15.29	2.24
Residual Paraffin	1	−30.4 (−143)††	–
Water Samples			
Shallow ground water, location 19	1	−7.14	–
Tensleep Formation water 72 TPX-10X	1	0.06	–

*Data from one location were not used because of probable breath contamination.
**One sample was discarded because of contamination with vegetation.
†Data from location 9 were not used.
††δD for residual paraffin.

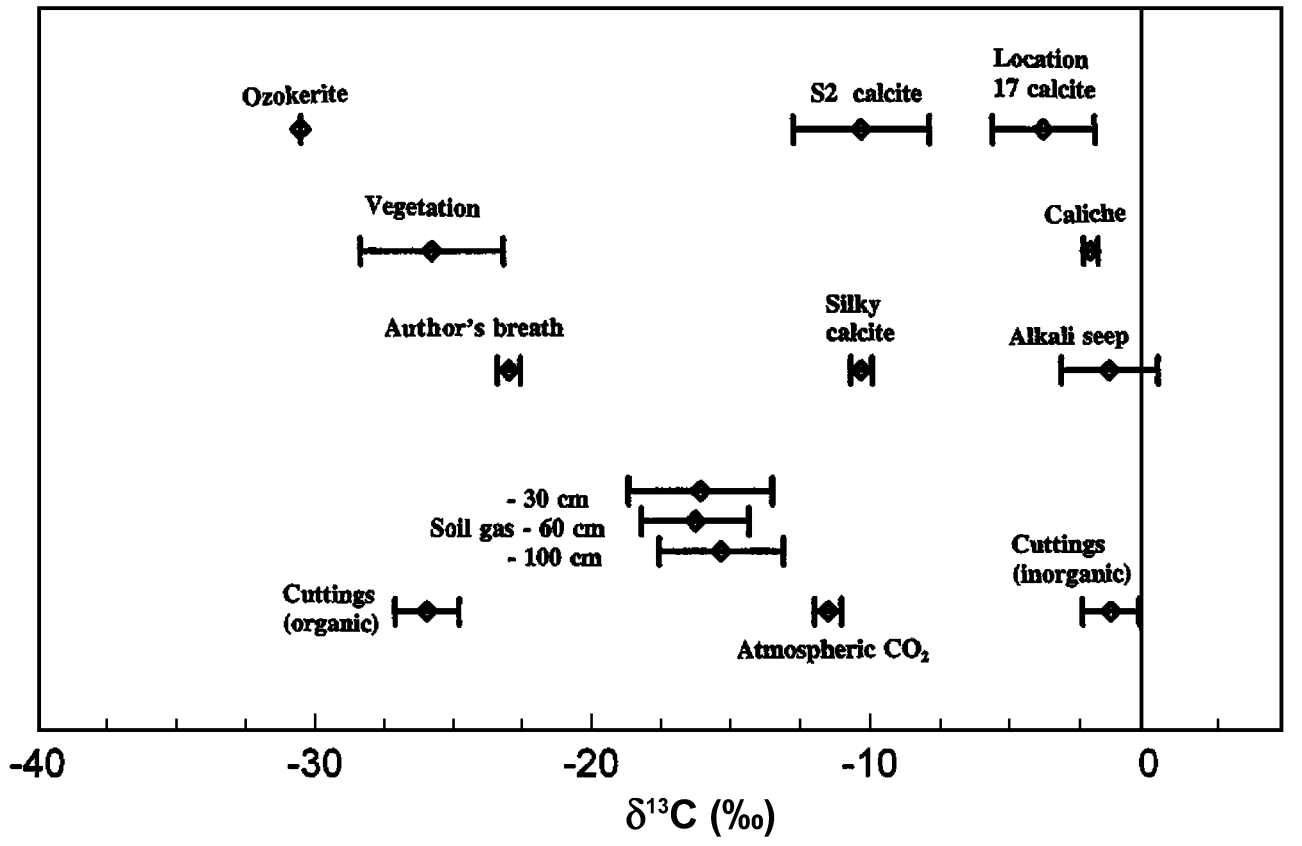

Figure 18. Simple isotopic shift model for carbon, using carbon isotopic data presented in Table 9.

APPENDIX: TEAPOT, WINTER 2004 SOIL-GAS FLUX AND CONCENTRATION DATA

	Latitude			Longitude			CO_2 Flux (mg m^{-2} day^{-1})	CH_4 Flux (mg m^{-2} day^{-1})	CO_2 (ppmv)	$\delta^{13}C_{CO_2}$ (‰)	CH_4 (ppmv)
Location	Degrees	Minutes	Seconds	Degrees	Minutes	Seconds					
1	43	20	3.7	106	13	18.4	254.98	0.166	611	−16.0	0.772
2	43	19	41.3	106	12	44.7	116.18	−0.435	401	−16.3	0.779
3	43	19	59.0	106	14	4.6	208.79	0.179	446	−14.5	0.975
4	43	19	23.8	106	13	44.5	131.32	0.209	421	−14.6	0.966
5	43	19	6.7	106	13	11.8	273.05	0.802	1484	−15.3	0.847
6	43	19	11.2	106	12	36.6	430.37	0.570	638	−13.6	0.993
7	43	18	39.5	106	12	17.9	676.48	−0.481	529	−12.5	0.995
8	43	18	34.5	106	12	48.8	153.54	0.403	431	−15.3	0.830
9*	43	18	34.6	106	12	57.3	1154.07	0.494	1562	−21.6	>8.77
10	43	18	27.4	106	13	18.2	131.46	0.352	432	−11.7	0.720
11	43	18	12.9	106	13	35.0	19.86	0.073	1148	−14.5	0.989
12	43	18	4.8	106	13	8.1	288.56	0.532	962	−17.8	1.008
13	43	18	43.9	106	13	51.2	303.39	−0.111	901	−17.5	0.917
14	43	18	43.8	106	13	46.5	−0.02	0.270	713	−14.3	1.006
15	43	18	33.2	106	13	49.4	300.08	−0.123	407	−14.6	0.957
16	43	17	27.7	106	12	53.6	76.56	0.311	1077	−14.0	0.996
17	43	17	23.2	106	12	35.0	41.46	−0.212	393	−12.3	0.986
18	43	17	40.0	106	12	6.9	732.91	−0.090	7783	−9.0	0.837
19	43	18	18.3	106	12	1.2	−281.70	−0.220	497	−16.6	1.102
20	43	18	37.2	106	11	46.1	430.87	0.014	622	−15.9	0.952
21	43	18	4.1	106	11	35.9	47.07	−0.122	602	−12.9	0.898
22	43	17	36.3	106	11	31.7	249.25	−0.061	591	−16.3	0.833

APPENDIX: Continued

Location	Latitude			Longitude			CO_2 Flux (mg m^{-2} day^{-1})	CH_4 Flux (mg m^{-2} day^{-1})	CO_2 (ppmv)	$\delta^{13}C_{CO_2}$ (‰)	CH_4 (ppmv)
	Degrees	Minutes	Seconds	Degrees	Minutes	Seconds					
23	43	17	34.0	106	10	48.9	328.58	−0.144	1988	−19.7	0.956
24	43	17	6.4	106	10	51.9	201.04	0.147	561	−16.4	0.930
25	43	17	9.1	106	11	22.5	332.11	0.244	813	−16.8	1.007
26	43	17	20.9	106	11	42.0	559.99	0.055	685	−12.1	0.970
27	43	17	16.7	106	12	16.0	101.66	−0.278	884	−16.3	0.972
28	43	16	52.5	106	12	44.0	372.04	0.055	735	−16.1	0.961
29	43	16	22.4	106	12	26.0	233.25	0.163	1052	−15.4	0.916
30	43	16	37.0	106	12	13.7	203.20	0.084	1562	−19.7	0.889
31	43	16	45.8	106	11	29.7	46.28	0.102	1280	−17.2	0.888
32	43	16	23.1	106	11	16.2	260.65	−0.013	700	−16.2	0.964
33	43	15	56.9	106	11	31.8	70.17	1.139	545	−16.4	0.627
34	43	16	28.2	106	10	52.2	320.15	0.057	1826	−18.5	0.908
35	43	15	57.5	106	10	34.7	65.14	0.286	1010	−16.1	1.001
36	43	15	35.8	106	11	0.6	214.07	0.372	725	−15.8	0.971
37	43	15	1.1	106	10	53.2	286.94	0.450	871	−15.1	0.853
38	43	14	55.5	106	11	23.7	194.76	0.229	1096	−17.8	0.911
39	43	15	28.7	106	12	2.5	341.43	−0.199	869	−13.3	1.036
40	43	16	2.5	106	12	3.3	139.80	0.585	508	−12.0	0.871

*Location 9 was contaminated, and the data were not used in the interpretation.

in a nested sampling system. These samples will be more thoroughly characterized compositionally and isotopically.

REFERENCES CITED

Bachu, S., 2000, Sequestration of CO_2 in geological media: Criteria and approach for site selection in response to climate change: Energy Conversion and Management, v. 42, p. 953–970.

Bachu, S., 2002, Sequestration of CO_2 in geological media in response to climate change: Road map for site selection using the transform of the geological space into the CO_2 phase space: Energy Conversion and Management, v. 43, p. 87–102.

Bachu, S., W. D. Gunter, and E. H. Perkins, 1994, Aquifer disposal of CO_2: Hydrodynamic and mineral trapping: Energy Conversion and Management, v. 35, p. 55–68.

Blunt, M., F. J. Fayers, and F. M. Orr, 1993, Carbon dioxide in enhanced oil recovery: Energy Conversion and Management, v. 34, p. 1197–1204.

Evans, D., 1965, Gas movement, *in* C. A. Black, D. D. Evans, J. L. White, L. E. Ensminger, and F. E. Clark, eds., Methods of soil analysis—Part 1: Madison, Wisconsin, American Society of Agronomy, Agronomy, v. 9, p. 319–330.

Hitchon, B., W. D. Gunter, T. Gentzis, and R. T. Bailey, 1999, Sedimentary basins and greenhouse gases: A serendipitous association: Energy Conversion and Management, v. 40, p. 825–843.

Klusman, R. W., 2003a, Rate measurements and detection of gas microseepage to the atmosphere from an enhanced oil recovery/sequestration project; Rangely, Colorado, U.S.A.: Applied Geochemistry, v. 18, p. 1825–1838.

Klusman, R. W., 2003b, A geochemical perspective and assessment of leakage potential for a mature carbon dioxide EOR project, and as a prototype for carbon dioxide sequestration; Rangely field, Colorado, U.S.A.: AAPG Bulletin, v. 87, p. 1485–1507.

Klusman, R. W., 2004, Naval Petroleum Reserve no. 3 CO_2 storage test site soil gas baseline studies: Annual report: Casper, Wyoming, Rocky Mountain Oilfield Testing Center, 98 p.

Klusman, R. W., M. E. Leopold, and M. P. LeRoy, 2000, Seasonal variation in methane fluxes from sedimentary basins to the atmosphere: Results from chamber measurements and modeling of transport from deep sources: Journal of Geophysical Research, v. 105D, p. 24,661–24,670.

Korbol, R., and A. Kaddour, 1995, Sleipner Vest disposal—Injection of removed CO_2 into the Utsira Formation: Energy Conversion and Management, v. 36, p. 509–512.

Landes, K. K., 1970, Petroleum geology of the United States: New York, Wiley-Interscience, 571 p.

McCutcheon, T. J., 2003, Time structure maps: 3D seismic data interpretation: Teapot Dome oil field, Naval Petroleum Reserve Number 3, Natrona County, Wyoming: Casper, Wyoming, Rocky Mountain Oilfield Testing Center, 7 p.

Thom Jr., W. T., and E. M. Spieker, 1931, The significance of geologic conditions in Naval Petroleum Reserve No. 3, Wyoming: U.S. Geological Survey Professional Paper 163, 64 p.

van der Meer, L. G. H., 1993, The conditions limiting CO_2 storage in aquifers: Energy Conversion and Management, v. 34, p. 959–966.

van Engelenburg, R. C. W., and K. Blok, 1993, Disposal of carbon dioxide in permeable underground layers: A feasible option?: Climate Change, v. 23, p. 55–68.

Weitz, J. L., and S. A. Harbison, 1954, Geologic map of Natrona County, Wyoming: U.S. Geological Survey and Wyoming State Geological Survey, Map G4263 N3 C5 1954, scale 1:158,000, 1 sheet.